UNIVERSIDAD DE INVESTIGACIÓN DE TECNOLOGÍA EXPERIMENTAL YACHAY TECH

Escuela de Ciencias Físicas y Nanotecnología

SYNTHESIS OF MAGNETIC NANOPARTICLES AND STUDY OF THE VARIATION IN COERCIVITY FIELD AS A FUNCTION OF PROPORTION BETWEEN SUPERPARAMAGMETIC TO BLOCKED NANOPARTICLES.

Trabajo de titulación presentado como requisito para la obtención del título de Ingeniero en Nanotecnología

Autor:

KEVIN RAÚL LANDÁZURI CORTEZ

kevinacho1428@gmail.com

Tutor:

Ph.D. WERNER BRAMER ESCAMILLA

wbramer@yachaytech.edu.ec

Cotutor:

Ph.D. SARAH BRICEÑO

sbricenio@yachaytech.edu.ec

Urcuquí, septiembre 2019

Urcuquí, 23 de agosto de 2019

SECRETARÍA GENERAL
(Vicerrectorado Académico/Cancillería)
ESCUELA DE CIENCIAS FÍSICAS Y NANOTECNOLOGÍA
CARRERA DE NANOTECNOLOGÍA
ACTA DE DEFENSA No. UITEY-PHY-2019-00015-AD

En la ciudad de San Miguel de Urcuquí, Provincia de Imbabura, a los 23 días del mes de agosto de 2019, a las 09:00 horas, en el Aula Sala Capitular de la Universidad de Investigación de Tecnología Experimental Yachay y ante el Tribunal Calificador, integrado por los docentes:

Presidente Tribunal de Defensa	Dra. GONZALEZ VASQUEZ, GEMA , Ph.D.
Miembro No Tutor	Dra. JANI MONA , Ph.D.
Tutor	Dr. BRAMER ESCAMILLA , WERNER , Ph.D.

Se presenta el(la) señor(ita) estudiante LANDAZURI CORTEZ, KEVIN RAUL, con cédula de identidad No. 0401722707, de la ESCUELA DE CIENCIAS FÍSICAS Y NANOTECNOLOGÍA, de la Carrera de NANOTECNOLOGÍA, aprobada por el Consejo de Educación Superior (CES), mediante Resolución RPC-SO-13-No.156-2015, con el objeto de rendir la sustentación de su trabajo de titulación denominado: Synthesis of magnetic nanoparticles and study of the variation in coercivity field as a function of proportion between superparamagnetic to blocked nanoparticles, previa a la obtención del título de INGENIERO/ A EN NANOTECNOLOGÍA.

El citado trabajo de titulación, fue debidamente aprobado por el(los) docente(s):

Tutor	Dr. BRAMER ESCAMILLA , WERNER , Ph.D.

Y recibió las observaciones de los otros miembros del Tribunal Calificador, las mismas que han sido incorporadas por el(la) estudiante.

Previamente cumplidos los requisitos legales y reglamentarios, el trabajo de titulación fue sustentado por el(la) estudiante y examinado por los miembros del Tribunal Calificador. Escuchada la sustentación del trabajo de titulación, que integró la exposición de el(la) estudiante sobre el contenido de la misma y las preguntas formuladas por los miembros del Tribunal, se califica la sustentación del trabajo de titulación con las siguientes calificaciones:

Tipo	Docente	Calificación
Miembro Tribunal De Defensa	Dra. JANI MONA , Ph.D.	8,5
Tutor	Dr. BRAMER ESCAMILLA , WERNER , Ph.D.	9,7
Presidente Tribunal De Defensa	Dra. GONZALEZ VASQUEZ, GEMA , Ph.D.	9,7

Lo que da un promedio de: 9.3 (Nueve punto Tres), sobre 10 (diez), equivalente a: APROBADO

Para constancia de lo actuado, firman los miembros del Tribunal Calificador, el/la estudiante y el/la secretario ad-hoc.

LANDAZURI CORTEZ, KEVIN RAUL
Estudiante

Dra. GONZÁLEZ VASQUEZ, GEMA , Ph.D.
Presidente Tribunal de Defensa

Dr. BRAMER ESCAMILLA , WERNER , Ph.D.
Tutor

Dra. JANI MONA , Ph.D.
Miembro No Tutor
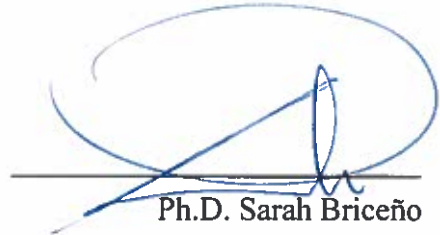
CIFUENTES TAFUR, EVELYN CAROLINA
Secretario Ad-hoc

CERTIFICACIÓN

Certificamos que el presente trabajo fue desarrollado por **KEVIN RAÚL LANDÁZURI CORTEZ,** bajo nuestra supervisión.

Ph.D. Werner Bramer Escamilla

TUTOR

Ph.D. Sarah Briceño

CO-TUTOR

AUTORÍA

Yo, **KEVIN RAÚL LANDÁZURI CORTEZ**, con CI 040172270-7 declaro que las ideas, juicios, valoraciones, interpretaciones, consultas bibliográficas, definiciones y conceptualizaciones expuestas en el presente trabajo; así cómo, los procedimientos y herramientas utilizadas en la investigación, son de absoluta responsabilidad del autor del trabajo de titulación. Así mismo, me acojo a los reglamentos internos de la universidad correspondientes a los temas de honestidad académica.

Kevin Raúl Landázuri Cortez

CI: 0401722707

AUTORIZACIÓN DE PUBLICACIÓN

"Yo KEVIN RAÚL LANDÁZURI CORTEZ cedo a la Universidad de Tecnología Experimental Yachay Tech, los derechos de publicación de la presente obra por un plazo máximo de cinco años, sin que deba haber un reconocimiento económico por este concepto. Declaro además que el texto del presente trabajo de titulación no podrá ser cedido a ninguna empresa editorial para su publicación u otros fines, sin contar previamente con la autorización escrita de la universidad"

Urcuquí, Septiembre de 2019

Kevin Raúl Landázuri Cortez

CI: 0401722707

Acknowledgements

Abstract

The subsequent thesis project presents a synthesis of magnetite nanoparticles Fe_3O_4 by co-precipitation method, its magnetic properties as a function of proportion are studied, which regards on a set of magnetite nanoparticles mixtures, superparamagnetic as well as blocked state magnetic nanoparticles were synthesized in order to perform the mixtures. The nucleus of the herein work lies on measuring/studying the change on coercivity field by changing the proportion of magnetite mass. The characterization involves techniques as: SEM, to obtain the morphology of the surface and VSM to study the magnetic properties of magnetite nanoparticles. The mixtures provide magnetic results as wasp-waisted and potbellied hysteresis loops, most of the results are explained in terms of mixtures between single-domain nanoparticles and samples containing multi-domain/single-domain particles. The variation of the magnetic properties is widely studied in the field of magnetic-recording devices or nano-devices in an electronic-magnetic component.

Keywords: *co-precipitation, hysteresis, potbellies, wasp-waisted, single-domain*

Resumen

El presente proyecto de tesis sintetiza la síntesis de nanopartículas de magnetita (Fe_3O_4) mediante el método de co-precipitación química, las propiedades magneticas de dichas nanopartículas son estudiandas en función a la proporción, la cuál consiste en un set de mezclas de nanopartículas de diferentes tamaños, el comportamiento magnético prominente en las nanoparticulas es superparamagnetismo y estado bloqueado. El núcleo del presente trabajo, radica en la medida/estudio del cambio en el campo coercitivo consequente al cambio de la masa en la proporción de nanopartículas. La sección de caracterización acogió tecnicas como SEM, para obtener la morfología y superficie, mientras que VSM, para estudiar las propiedades magnéticas. Las mezclas arrojaron resultados como hysteresis wasp-waisted y potbellied, la mayoría de los resultados son explicados en términos de las mezclas entre partículas single-domain y single-domain/multi-domain. La variación en las propiedades magnéticas es ampliamente estudiado en el campo de dispositivos de almacenamiento magnético o nano-dispositivos en el componente electrónico-magnético.

Palabras clave: *co-precipitación, hysteresis, potbellied, wasp-waisted, dominio-simple, multidominio, magnetita*

Contents

List of Figures

List of Tables

Chapter 1

Introduction

Magnetite is a mineral commonly found in nature which belongs to the oxides of iron, its chemical formula is $Fe^{3+}(Fe^{3+}, Fe^{2+})O_4$. These minerals presents a huge spectrum of applications in its bulk material as well as in its nanometric size. Magnetite Fe_3O_4 in its nanometric scale, as well as any other material, differs in its electrical, optical, chemical and magnetic properties from bulk size, this is the reason why magnetic nanoparticles (MNPs) have acquired great interest on biomedical[1], magnetic-recording devices[2] and ferrofluid[3] fields. MNPs have a large surface-to-volume radio and high surface energies, thereby they tend to aggregate to reduce the surface energies, for this reason the control size synthesis of magnetite nanoparticles faces a technological challenge[4].

Ferromagnetism is a principle of magnetic materials to form permanent magnets, the ferromagnetic particles consist of a single domain until a critical particle size is reached as *Frenkel and Dorman*[5] predicted. In other words once the size of a ferromagnetic material is reduced below a certain critical value, the behavior of particle becomes single domain. The magnetic domains, are regions where the magnetic moments μ are aligned in the same direction by exchanging forces known as uniform magnetization. By applying a external magnetic field (H) to a ferromagnetic material, the reaction will produce a hysteresis loop, such loop is characterized by two parameters: remanence and coercivity. The coercivity H_c, which is the main focus of the present thesis project, is related with the 'thickness' of the curve and it has a strong dependence on size particle. **Figure**1.1 shows how the coercivity reaches a maximum when the particle size is reduced, after that this coercivity decreases toward zero[6].

The experimental critical particle size of a ferromagnet reaches an approximate radius of 15 nm by taking the particle as an sphere. Regarding the single-domain (SD) nanoparticles, *Stoner and Wohlfarth*[7] proposed a mechanism of magnetization reversal in SD nanoparticles, this model consists on inducing a magnetization reversal by the rotation of the magnetization vector from the easy axis to another. Thereby, the rotation mechanism affects to the coercivities of MNPs[8].

Considering a system of non-interacting SD particles practically isolated, the magnetic moments of each particle
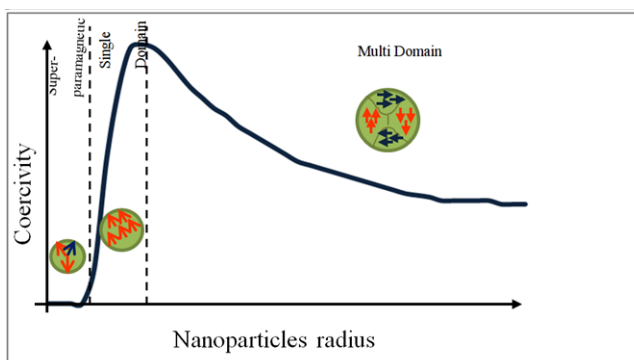
Figure 1.1: Coercivity behavior as a function of size particle.

will act separately. Those particles are conditioned by the thermal agitation which conducts to a magnetic instability, thereby the superparamagnetism (SPM) effect occurs. SPM depends on particle radius as is shown in **Figure**1.1, then as the radius decreases the superparamagnetic effect is prominent, also the coercivity becomes zero, thereby it is not possible to have hysteresis, so that the nanoparticles become magnetic in the presence of an external magnetic field (magnet), but revert to a nonmagnetic state instantaneously as the magnet is retired.[6].

Even if the magnetic behaviour of nanoparticles may be different (superparamagnetism, ferromagnetism, ferrimagnetism), it is possible to mix those nanoparticles with different magnetic response, as *Bean* did it in 1955, in order to obtain a new/different magnetic behaviour, depending on the proportion in mass of the mixtures, the magnetic hysteresis loops will change, normally the mixtures are based on a set of single-domain particles mixed with multi-domain/blocked particles.

The present thesis basically relates the synthesis and magnetic study of magnetite nanoparticles, in the first part of the thesis, we have synthesized a set of five different size nanoparticles of Fe_3O_4 by controlling its size by the co-precipitation method, the parameters controlled in such method are time of reaction and time of calcination. To reach a non-interacting assembly of nanoparticles, polyvinil alcohol (PVA) was used in order to avoid agglomeration by covering the nanoparticles. Once we had the five different average size nanoparticles, we proceeded with the mixture process, which consists on mixing different powders, in our case we worked with two of the five samples previously prepared in different proportions, due to study and compare two different magnetic behaviour.

The second part of the thesis relies on applying morphological and magnetic characterization to the final samples lately named, the structural part will be provided by the scanning electron microscopy (SEM) whereas the magnetic one was taken from vibrating sample magnetometer (VSM).

Finally, the third and last part of the present thesis is based on the results of VSM, which provide us variations

on coercive field as a function of the different proportions of nanoparticles with different sizes, in this chapter the results are studied and analyzed by comparing it with the literature reported ones.

1.1   Problem statement

The change in coercive field as a function of the ratio of mixtures between super-paramagnetic and blocked magnetite nanoparticles.

The variation of coercive field in different types of material like geological magnetic minerals or synthesized nano-particles, can be physically explained due to a phenomena related with a mixture between populations of superparamagnetic particles (SP) and blocked nanoparticles (BP). The change on coercivity normally depends on the variation of the ratio between SP-BP; as the size of particles increases, the blocked behavior is prominent, contrastingly when such size is decreased the particles tend to superparamagnetism. Furthermore, the change in coercivity can produce a distortion in the shape of the magnetic hysteresis, giving two types of behavior one is the wasp-waisted (constricted middles), and finally the potbellies (slouching shoulders)[9].

1.2   General and Specific Objectives

1.2.1   General Objectives

Synthesis of magnetite nanoparticles by co-precipitation method, and study the variation in the coercivity field as a function of proportion between superparamagnetic to blocked magnetite nanoparticles.

1.2.2   Specific Objectives

1. Synthesis of magnetite nanoparticles using the co-precipitation method.

2. Change the synthesis parameters to modify the average size of the nanoparticles.

3. Structural and Magnetic characterization of samples using SEM and VSM respectively.

4. Mix the nanoparticles as a function of the proportion between superparamagnetic to blocked nanoparticles to study the variation in the coercivity field.

Chapter 2

Theoretical Background

The first part of the present chapter study the magnetic nanoparticles (MNPs), its properties and magnetic behaviour, by discussing the superparamagnetic effect. Furthermore, anisotropy contributions are studied in the nanoparticle system. Additionally, the concepts of Potbellies and Wasp-waists are introduced by studying the hysteresis loops in magnetic nanoparticles assembles found in nature as well as simulations. Finally, the coercive field change as a function of particle size is discussed with the hand of partial mixtures with different size distributions.

In the other hand, the second and third parts brings together the fundamentals of magnetite nanoparticles synthesis and characterization. Co-precipitation method is widely used to synthesize magnetite nanoparticles, thereby its working principle is explained. To characterize the samples, SEM and VSM techniques are described.

2.1 Magnetism

Magnetic nanoparticles spectrum of applications strongly depends on the interesting properties that such material display, to analyze the magnetic properties is important to point out the crystalline formation of magnetite from iron atoms or $Fe^{3+} and Fe^{2+}$, because the particles can be in ferromagnetic, antiferromagnetic or ferrimagnetic states. The different states are shown in **Figure**2.1.

The first state that appears in **Figure**2.1 is known as paramagnetism, some materials exhibit paramagnetism due to atoms or ions present a net magnetic moment and it is due to unpaired electrons in partially filled orbitals, as Iron, in this state all the magnetic moments μ are oriented in a random way, consequently the crystal has not net magnetic moment, in other words, the net magnetic moment is zero. The unique way to increase or decrease the net magnetic moment elicits through applying an external magnetic field.

Ferromagnetic bulk materials exhibit very strong interactions between their magnetic moments, those interactions are generated due to a quantum mechanical phenomenon known as electronic exchange forces, resulting in parallel alignment of moments, as is shown in **Figure**2.1, such effect will produce large net magnetization even if the material

Paramagnetism

Ferromagnetism   Antiferromagnetism   Ferrimagnetism
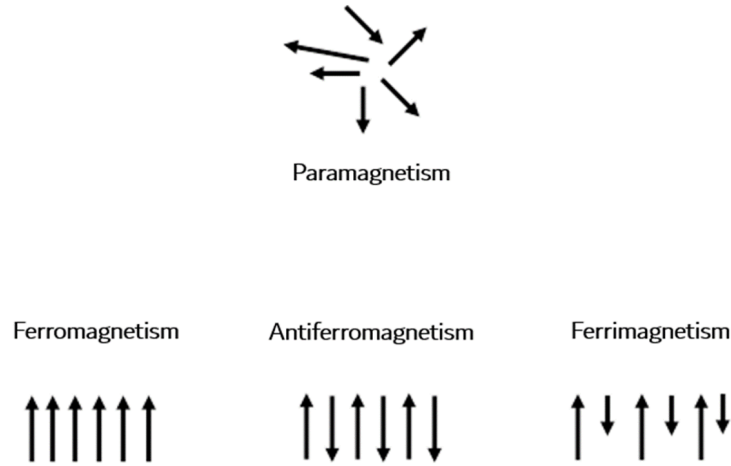
Figure 2.1: Different states depending of the magnetic moments alignment.

is not subjected to a external magnetic field. In the latter case, the magnetization M can be measured as a function of an external field H, so that hysteresis loops are betrayed. *Pierre Weiss* in 1907 proposed a model in order to explain the hysteresis behaviour by assuming that ferromagnetic materials are constituted by domains.[10]. Such domains are distanced by domain walls, generally described as topological solution, in the case where a discrete symmetry is spontaneously broken[11]. Furthermore, the magnetostatic energy given by $2\pi N_{ij} \mathbf{M_i M_j}$, increases as the volume of the material increases too, whereas the domain wall energy increases proportionally to the surface area. The coefficients N_{ij} are known as the demagnetization coefficients which depends on the shape of a ferromagnetic material and $\mathbf{M_i M_j}$ are the components of the magnetization M. At certain point, the formation of domains becomes unstable, therefore the sample consists on a single-domain (SD), which is basically the principle of small permanent magnets, this point is achieved when the critical radius r_c does not overcome the r_c given by **Eq**2.1.[12]

$$r_c \approx 9 \frac{(AK_\mu)^{\frac{1}{2}}}{\mu_0 M_s^2} \tag{2.1}$$

where A is the exchange constant, K_μ is known as the uniaxial anisotropy constant, μ_0 the general constant of permeability, and M_s is the saturation magnetization.[8]

Temperature dependence in paramagnetic states is very important; **Figure**2.1 shows a three different route of states: ferromagnetic, antiferromagnetic and ferrimagnetic. When the temperature is increased, the ordered arrangement of magnetic moments decreases due to thermal fluctuations. So that, overcoming the Curie temperature T_C, the state is ferromagnetic or ferrimagnetic; in the same way, beyond the Neél temperature T_N the state is antiferromagnetic.

Ferrimagnetic materials, in contrast to ferromagnetic ones, are generally ionic compounds such as iron oxides, the magnetic spins in a ferromagnetic oxide is shown in **Figure**2.2. Basically, the magnetic structure strongly depends on
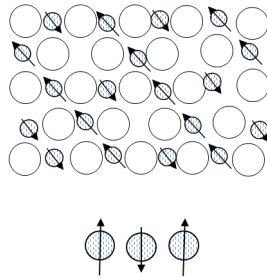
Figure 2.2: Magnetic structure of a ferrimagnetic oxide.
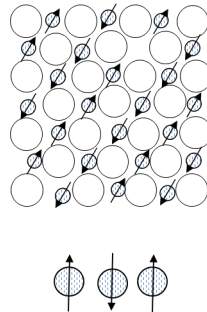
Figure 2.3: Magnetic structure of antiferromagnetic materials.

two magnetic sublattices *A* and *B* separated by oxygen atoms. In this system, the exchanges forces are controlled by the oxygen anions, therefore those interactions are called indirect or superexchange interactions (SPI). The strongest SPI turns out in an antiparallel alignment of spins between the sublattices A and B, as is shown in **Figure**2.2. As we can notice, the magnetic moments of A and B sublattices are different either in direction and magnitude. It is possible to state that ferrimagnetism has many similarities with ferromagnetism such as spontaneous magnetization, hysteresis and remanence.[13] Magnetite, which is the central point of this thesis, exhibits ferrimagnetism as is explained by *Banerjee. S. and Moskowitz B.* in 1985.[14]

Antiferromagnetism, in the other hand, contains sublattice A and B as well as the ferrimagnetism and ferromagnetism, the difference roots in the magnetic moments of each sublattice, in the antiferromagnetism case, the magnetic moment is exactly equal but with opposite direction **Figure**2.3, which leads to have a zero net moment.

2.1.1 Hysteresis Loop

Since ferromagnetic/ferrimagnetic materials can be highly magnetized by an external magnetic field, there are changes on magnetization of the material that depends on the external applied magnetic field, this can be notice in
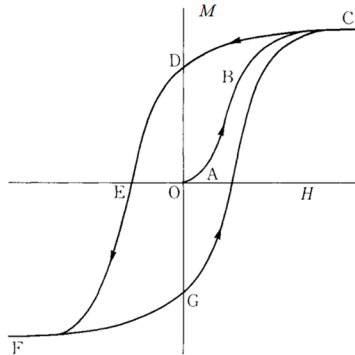
Figure 2.4: Schematic representation of hysteresis loop. [15]

Figure2.4. The O point, is called demagnetized state where magnetization, M, as well as applied field, H, are zero. After that, the magnetization grows as magnetic field M increases along the curve $OABC$, due to the material gets magnetized and the magnetization value represents how much magnetic remanence possesses the material after the applied H, the latter point is known as saturation magnetization (M_s). In a certain region as OA, the magnetization can be considered as reversible by removing the magnetic field, so then the magnetization returns to zero. Normally the slope between A and B is called *initial susceptibility* x_a. Once the curve exceeds the point B, the magnetization is no longer reversible.[15]

Once the magnetic field reaches its saturation point C **Figure**2.4, it will decrease gradually along CD instead of going $CBAO$, then at the $H = 0$ point, the value of M is not zero, but *residual magnetization* or the remanence (M_r) that is D point. To achieve M to be zero, the magnetic field might be increased in the negative direction. The OE portion is called the *coercive field* (h_c) . Furthermore, the negative increasing of H until F point, concludes with the negative saturation magnetization. Finally the closed loop $CDEFGC$ is the widely known *hysteresis loop*.[15]

2.1.2   Magnetism in Nanoparticles

Nanomagnetism or magnetism in nanoparticles is a topic widely studied due to its possibility to modify in certain way the magnetic properties of nanoparticles, some of the most important consideration to study the magnetic properties such as the coercivity (H_c), saturation magnetization (M_s) and remanent magnetization (M_r) are the particle size and domain structure. In the case of M_s, it will increase as the size particle does, this case is independent of crystal structure or particle shape. In the other cases M_r and H_c it is needed to establish a limit known as superparamagnetic limit, normally when the size particle becomes too small around 25 nm, the limit is present (in some applications as magnetic recording devices, nanoparticles need to beat the superparamagnetic limit). Then, when the superparamagnetic limit is exceeded, the M_r and H_c values increases as well as the particle size, until it reaches a critical size where a transition from mono-domain structure to multi-domain structure occurs. Above the critical size, the M_r
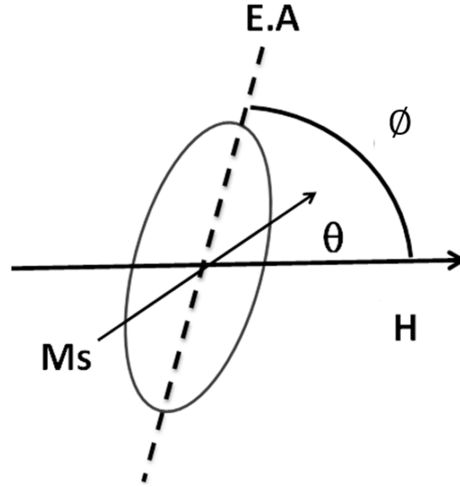
Figure 2.5: Single domain grain with the magnetization M and the external applied magnetic H, ϕ is the angle at H field is externally applied.

and H_c values decreases as it is illustrated in **Figure**1.1. [16,17]

The magnetism of nanoparticles can be explained by using the Stoner and Wohlfarth (SW) model. In 1948, SW proposed a model [7] to explain the magnetization reversal in single domain nanoparticles. The model considers a ferromagnetic/ferrimagnetic material with a single magnetic moment (SD), normally small grains containing about 10^{12} - 10^{18} atoms. The SW model purpose is to describe the magnetization curves of such aggregation of SD particles, which present uniaxial anisotropy, this anisotropy is characterized by an axis where the magnetization M prioritises to lie in order to minimize the energy [18]. There are two general assumptions of the model: coherent rotation of magnetization (all spins of the system are parallel to respect to each other) and negligible interaction between particles [8].

Figure2.5 shows the system of variables for the SW model. When an external magnetic field H is applied to this system, there will be an angle that determines the direction of magnetization relative to the easy axis, this angle is known as (θ), and it will fix the equilibrium direction of the magnetization vector [8]. Thus, the magnetization vector is subjected to two energies such that the density energy of the system can be written in terms of anisotropy (E_A) and Zeeman energies ($E_z = -M \cdot H$) as is shown in the **Eq.**2.2. At T=0K, the total energy of the system is then:

$$E = E_A + E_Z = K \sin^2(\theta) - \mu_0 H M_S \cos(\phi - \theta) \tag{2.2}$$

Getting the derivative of the energy equation 2.2 with respect to the angle θ, and equall to zero, we obtain:

$$\frac{dE}{d\theta} = 2K \sin\theta \cos\theta - \mu_0 H M_S \sin(\phi - \theta) = 0 \tag{2.3}$$

Which provides the equilibrium position of M, and magnetization resolved in field direction is given by:

$$M = M_S \cos(\phi - \theta) \tag{2.4}$$

Equation 2.3 is then:

$$2K \sin\theta \cos\theta = \mu_0 H M_S \sin(\psi - \theta) \tag{2.5}$$

One important case to analyze consists on considering the magnetic applied field to be normal to the easy axis, which implies $\psi = 90^o$. So that, by applying trigonometric relations $\sin(x - y) = \sin(x)\cos(y) - \cos(x)\sin(y)$ and $\cos(x - y) = \cos(x)\cos(y) + \sin(x)\sin(y)$ to equations 2.5 and 2.4 respectively, we obtain:

$$2K \sin(\theta) \cos(\theta) = \mu_0 H M_s \cos\theta \tag{2.6}$$

and,

$$M = M_s \sin(\theta) \tag{2.7}$$

$$\sin(\theta) = \frac{M}{M_s} \tag{2.8}$$

Plugging 2.8 in to 2.6 and cancelling $\cos(\theta)$, we obtain:

$$2K \frac{M}{M_s} = \mu_0 H M_s \tag{2.9}$$

Let m be the reduced magnetization, such that $m = M/M_s$, finally:

$$m = \mu_0 H \left(\frac{M_s}{2K}\right) \tag{2.10}$$

Thinking in terms of hysteresis, equation 2.10 provide us an interpretation where magnetization will be linear as a function of H, such that there is not hysteresis loop, instead the plot of such hysteresis is linear.

The saturation state is easily explained by the assumption of ferromagnetic/ferrimagnetic materials to have magnetic domains, before applying an external magnetic field with random orientation, cancelling each other producing a net external magnetic field almost negligibly; after applied magnetic field, those domains are aligned parallel to such field, triggering a large magnetic field B, at certain point, almost all the magnetic domains are totally aligned so any increment in the applied field will not cause major alignment, and the magnetization remains nearly constant, this point is known as saturation point[19].

The conditions to reach saturation under the current model, is that magnetic field applied $H = H_k = 2K_u/M_s = $ *uniaxial anisotropy field*. Let h be the reduced field, such that $h = H/H_k = 2K_u/M_s$, then:

$$h = \left(\frac{H}{H_k}\right) = \mu_0 H\left(\frac{M_s}{2K_u}\right) \tag{2.11}$$

In the case of $\psi = 90^o$, m is equall to h, and then Eqs. 2.3 and 2.4 can be written as

$$\sin(\theta)\cos(\theta) - h\sin(\psi - \theta) = 0 \tag{2.12}$$

$$m = \cos(\psi - \theta) \tag{2.13}$$

Another important case to consider is when the magnetic field is along the easy axis, which implies $\psi = 0^o$. Two states can be reached, H reduced to $\psi = 0^o$ and increased negatively to $\psi = 180^o$. In both situations, H and M_s are perpendicular; furthermore, when H reaches high values in negative orientation a phenomenon of "flip over" occurs with the magnetization, from $\theta = 0^o$ (where magnetization is unstable) to $\theta = 180^o$ (parallel to H).

The second derivative of the total energy E, will give us the equilibrium energy states by equating this one to zero. Then, this derivative is:

$$\frac{d^2 E}{d\theta^2} = 2K(\cos^2(\theta) - \sin^2(\theta) + \mu_0 HM_S(\cos(\psi - \theta)) = 0 \tag{2.14}$$

Dividing both sides by $2K_u$ we obtain:

$$\frac{1}{2K_u}\frac{d^2 E}{d\theta^2} = (\cos^2(\theta) - \sin^2(\theta) + h(\cos(\psi - \theta)) \tag{2.15}$$

From equation 2.15 is possible to notice the sign of $\frac{d^2 E}{d\theta^2}$, when it is positive that means the equilibrium is stable, otherwise the equilibrium is unstable; furthermore, if it is zero, the meaning is related with the change of stability to a unstable position[8].

Finally, the solutions of Eqs. 2.12 and 2.15 give us values of critical field h_c and critical angle θ_c as *Bedanta* calculated in its study[8], the solutions are shown below:

$$\tan^3(\theta_c) = -\tan(\psi) \tag{2.16}$$

and,

$$h_c^2 = 1 - \frac{3}{4}\sin^2(2\theta_c) \tag{2.17}$$

Figure 2.6 shows the hysteresis loops of an assembly of non-interacting particles calculated for different values of ψ, for example when $\psi = 180^o$, $\theta_c = 0$ and $h_c = 1$ which produces a hysteresis loop rectangular as the first case in **Figure** 2.6, further values are calculated in order to vary the shape of the hysteresis as a function of the angle of applied magnetic field. *

---

*Some calculations and interpretations were followed in the PhD thesis of *Bedanta, Subhankar* in 2006[8]
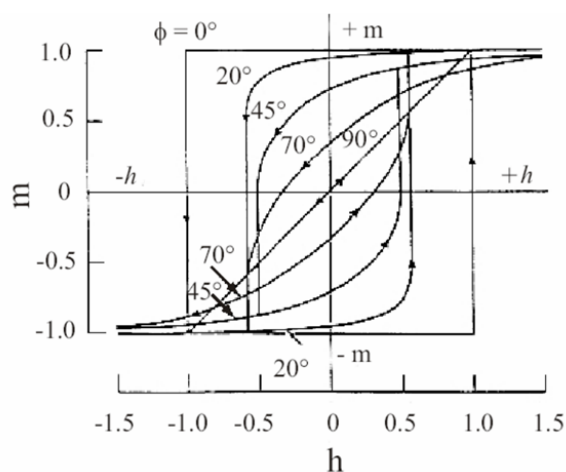
Figure 2.6: Hysteresis curve of SD particles with different angles between anisotropy axis and external field. [7]

Exchange bias in core-shell model

It is know that monodomain nanoparticles also have a complex internal structure. One morphological structure of a nanoparticle is based on the assumption of the existence of an intrinsic surface structured disorder layer that propagates until the center of the particle where the magnetic order prevails. In this situation, anisotropy varies with size in a non-linear way[20]. Furthermore, considering that nanoparticles are constituted by a core with some characteristic wrapped in a shell that have its own magnetic behaviour. A substantial difference appears between shell and core because those may present different material or in the case of same material they can present different phase or crystalline order. So that, such kind of nanoparticles can present a behaviour called exchange bias (EB), the consequence of this effect is a shift on the magnetization curve M-H, and also it can change the shape of the hysteresis. [21]

In the case of having core/shell nanoparticles, an phenomena known as exchange coupling appears across the core/shell interface, this coupling can be seen in a form of exchange bias, that is an effect which exhibits an exchange interaction between a hard magnetization from an antiferromagnetic (AFM) with the soft one from a ferromagnetic (FM)/ferrimagnetic (FIM) material at their interface[22]. In layers the effect is better didactic explained, first the material must be cooled through Neél temperature, an AFM acts as a pinning layer, thereby acquires unidirectional anisotropy. Those settings joined together lead to a hard switching in magnetization of the FM in the opposite direction of the cooling external field, so that a shift on the hysteresis loop is prominent and it is the result of the exchange bias effect. EB effect can be present in core/shell Fe_3O_4 nanoparticles and several studies have shown the shift on magnetization curve (M-H) for those specific nanoparticles. [23,24]

A simple but educational model for a nanoparticle with this type of structures is built by the assumption of two

magnetic moments M_1 and M_2, and both with different anisotropic parameter Ka_1 and Ka_2. Both M_1 and M_2 are coupled and the term used for this is given by Heisenberg coupling terms: $JM_1M_2cos(\phi)$, where J is the exchange coupling parameter between the to magnetic moments M_1 and M_2 and ψ is the angle among them. The energy for such system would be the addition of the coupling expression with **Eq.**2.2, for two magnetic moments, that is,

$$E = \sum_{i=1,2} Ka_i sin^2(\theta_i) - \mu_0 HM_i cos(\theta_1 - \theta_0) + JM_1M_2cos(\theta_1 - \theta_2) \tag{2.18}$$

here θ_1 and θ_2 are the angles between the external applied field H and the two magnetic moments M_1 and M_2.

This model can simulate in first approximation the magnetic behaviour of the nanoparticles synthesized in this work as it will be discussed in Results section.

2.1.3 Superparamagnetism

Once we defined the behaviour of SD nanoparticles, we can compare this SD with an atomic paramagnetism but with some exceptions as its extremely large moment and thereby large susceptibilities that are involved[25]. Considering the latter similarities and differences, the magnetic behaviour has been named *superparamagnetism*[26]. This interesting magnetic behaviour also was discussed in literature under different terms and definitions as *apparent paramagnetism*[27], *collective paramagnetism*(3nm)[28], *quasiparamagnetism*[29] and *subdomain behaviour*[30].

A SD magnetic material is considered to have a magnetic behaviour such as superparamagnetism, if it does not present hysteresis loop as is shown in **Figure**2.7, in the case of iron oxides ferrimagnetic nanoparticles reported by *Cornell et al.* in 2003[31], to be superparamagnetic, the iron oxide particles as the ones presented in the study of *Gupta A., and Gupta M. in 2004* might be monosized in the range of 6-15 nm because at this values the iron oxides nanoparticles are single-domain.[32]

In the SD ferromagnetic/ferrimagnetic systems, superparamagnetism is presented due to the thermal energy from the assemble of nanoparticles overcomes its anisotropic energy. The most understandable system to explain superparamagnetism, is given by *Bedanta, Subhankar* in 2006[8], such model parts by considering an assembly of non-interacting, uniaxial and SD particles, everyone carrying an anisotropy energy density as *Eq.*2.19:

$$E = KV \sin^2(\theta) \tag{2.19}$$

Where θ is the angle that the magnetization vector forms with the easy axis, K is the anisotropy energy density and V as the volume of the particle. For any particle, the energy barrier is $DE = E_B = E_{max} - Emin = KV$ and such energy carry off the two points at $\theta = 0$ and $\theta = \pi$ to the easy axis as is shown in **Figure** 2.8, the first energy minima $\theta = 0$ specifies the parallel direction of magnetization, whereas the anti-parallel one is given by $\theta = \pi$.
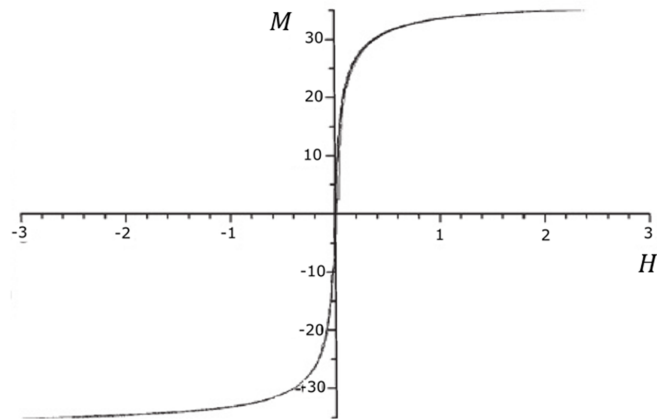
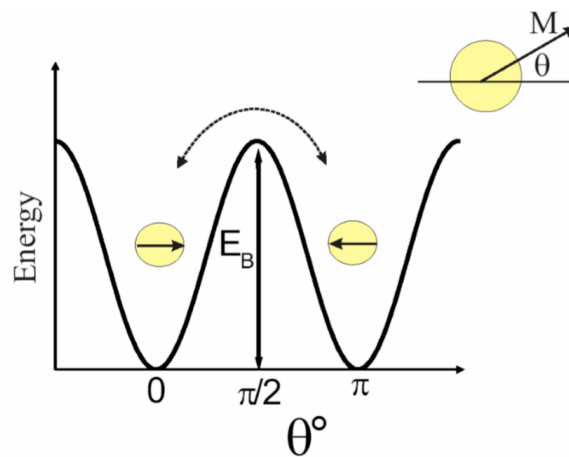Figure 2.7: M-H curve for a NP in Superparamagnetic state.

Figure 2.8: Representation of the energy of a SD particle with uniaxial anisotropy versus the magnetization direction. E_B represents the energy barrier to overcome in order to present rotation magnetization and q or θ is the angle that magnetization forms with the easy axis.[8]

In the case that KV is very small, which implies that the size of particles decreases too much, the KV would become so low that the energy fluctuations will be greater than the anisotropy energy, as *Néel* predicted, ending with a magnetization spontaneously reverse from one easy direction to the other, sometimes without the magnetic applied field.

Now, the system of non-interacting particles is studied under the assumption that all the particles are separated far enough so that there is not interaction between them. Furthermore, those particles are inside a non-magnetic matrix so that there are not magnetic contributions to the system. Then for $k_B T >> KV$, being the $k_B T$ Boltzmann constant and T temperature, the material is considered to be paramagnetic, the system change its magnetic behaviour when the independent moments are not considered the ones of independent atoms but a system with approximately 10^5 atoms, finally the latter system is considered **superparamagnetic**[8].

At finite temperature and applying enough energy to a system, the magnetization will flip over and reverse its direction along the easy axis, as we already explained, then the time known as *Néel relaxation time* τ_N takes place, and this time is given by the widely known *Néel-Arrhenius equation*:[33]

$$\tau_N = \tau_0 \cdot \exp \frac{KV}{k_B T} \tag{2.20}$$

Where τ_N is then the average length of time that magnetization of nanoparticles take to randomly flip as a result of thermal fluctuations, τ_0 is the inverse attempt frequency dependent on each material normally with values between $10^{-9} and 10^{-10}$, KV is the energy barrier, $k_B T$ are the Boltzmann constant and temperature respectively. At the moment where the thermal energy exceeds the energy barrier, superparamagnetic relaxation will occur, and superparamagnetic particles will be ordered below a blocking temperature, T_B .

Blocking Temperature T_B

Let us assume that the magnetization of a superparamagnetic particle is measured and its time measurement be τ_m. At low temperatures, there appears two cases: the first one involves the time of the magnetization measurements and it is much longer than the Néel relaxation time ($\tau_m >> \tau_N$) adding that there is not external field, the magnetization will flip several turns, so that its average magnetization seems to be zero[34]. In the other hand, if the measured relaxation time is less than the Néel's one ($\tau_m << \tau_N$), the magnetization will not flip in the measurements and it stays to be "blocked" in its initial state or at the beginning of taking measurements, in this former case, is valid to affirm that the particles are in a blocked state.

Both cases have been studied and in a certain point where ($\tau_m = \tau_N$), there suppose to appear a transition between superparamagnetic and blocked state and it is characterized by blocking temperature equation 2.21[35].

$$T_B = \frac{KV}{k_B \ln(\frac{\tau_m}{\tau_0})} \tag{2.21}$$

2.1.4   Wasp-Waisted Hysteresis Loops

Hysteresis loops on special occasions are different as the ones shown in **Figure** 2.4, instead there are wasp-waisted hysteresis loops (WWHL), a few studies have defined such hysteresis as: hysteresis loops that are constricted in the middle section, but are wider above and below the middle section[9,36], or hysteresis that whose width narrows as the magnetization goes to zero (middle) and then opens up again[37]. Those non-typical behaviours have been observed in different materials either natural (minerals) or synthesized[9,38–40]. In the case of minerals, it has been found submarine basaltic glass containing a low-titanium magnetite as the magnetic phase, to have a WWHL as is shown in **Figure** 2.9, which as the name suggest the curve of hysteresis appears to contract as the magnetization decreases at zero, after such change this loop grows as the applied field arises a saturation magnetization . Normally the WWHL found in nature belong to geological materials that comprises mixtures of magnetic minerals with different grain sizes[36].

Two general approaches can be taken in order to study WWHL, the first one relates the experimental research done in geological minerals mostly magnetic with different size distributions. Whereas the second one, relates simulations where different samples are mixed, there is an experiment done by *Wasilewski* in 1973[38], where it is possible to modify the normal hysteresis of magnetic materials by mixing up, in one specific case it is assumed two ferromagnetic/ferrimagnetic materials, in the former one the coercivity value is much longer than the latter one. Let us consider both materials as: A and B shown in **Figure** 2.10 [(a) and (b)]. There will be an antiferromagnetic coupling as shown in **Figure**2.10 [(c) and (d)]. So that, the addition of the loops that are part of the composite is the known as wasp-waist loop illustrated in **Figure**2.10 [(e)].[37]
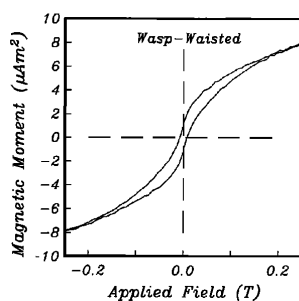
Figure 2.9: Wasp-waisted Hysteresis loop for submarine basaltic glasses. [9]

2.1.5   Potbellies

Potbellies are different variation in the shape of hysteresis loop, in contrast of wasp-waists, potbellies loops are distorted having slouching. In the same sense of generating wasp-waists, potbellies are easily generated from population of single-domain nanoparticles and superparamagnetic systems (SD/SP) or mixtures of various minerals, grain sizes and domain states.[9]
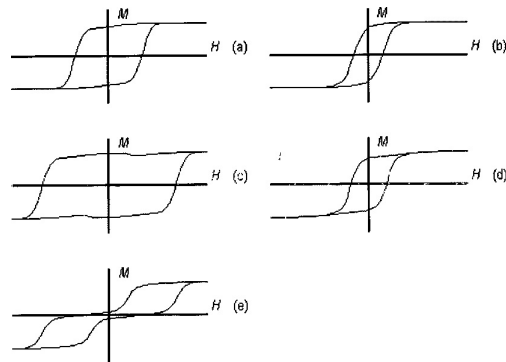
Figure 2.10: (a) Hysteresis loop of a FM material A, (b) hysteresis loop of FM material B, (c) result of antiferro-magnetic coupling between material A and B, (d) coupled loop from material B and (e) wasp-waist hysteresis loop from composite. [37]

The potbellied system from submarine basaltic glasses is shown in **Figure**2.11, by examination the shape of potbelly is possible to infer that the shape changes drastically to a normal hysteresis loop and a wasp-waisted loop, the most remarkable change appears at the zero point either in coercivity and remanence, so that the hysteresis loop grows its shape and it returns to its arm's point. In the same way that in WWHL, potbellies loops can also be obtained by considering two materials A and B, in this scenery the coercivities from A might be higher than B, as it is shown in **Figure** 2.12 [(a) and (b)], with a slightly difference, which is that material A has smaller switching field distribution than B, this effect is normally seen in single-domain systems, the switching field of the particles is in charge of producing remanent magnetization[41]. For each different particle, there is a specific switching field at which it reverses its state of magnetization[42]. So that, the 'creation' of a pot-bellied hysteresis loop is again based on an antiferromagnetic coupling between material A and B **Figure** 2.12 [(c) and (d)], and finally a the potbelly loop is obtained **Figure**2.12 [(e)]. [37]
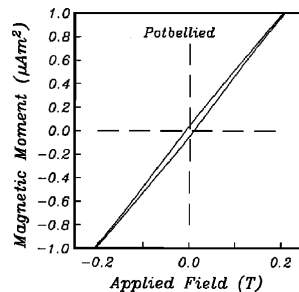
Figure 2.11: Hysteresis loop for submarine basaltic glasses. [9]
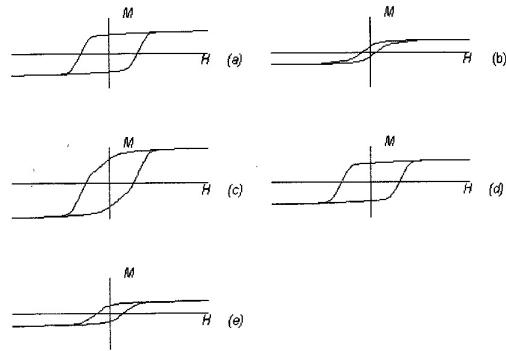
Figure 2.12: (a) Hysteresis loop of a FM material A, (b) hysteresis loop of FM material B, (c) result of antiferro-magnetic coupling between material A and B, (d) coupled loop from material B and (e) pot-bellied hysteresis loop from composite.[37]
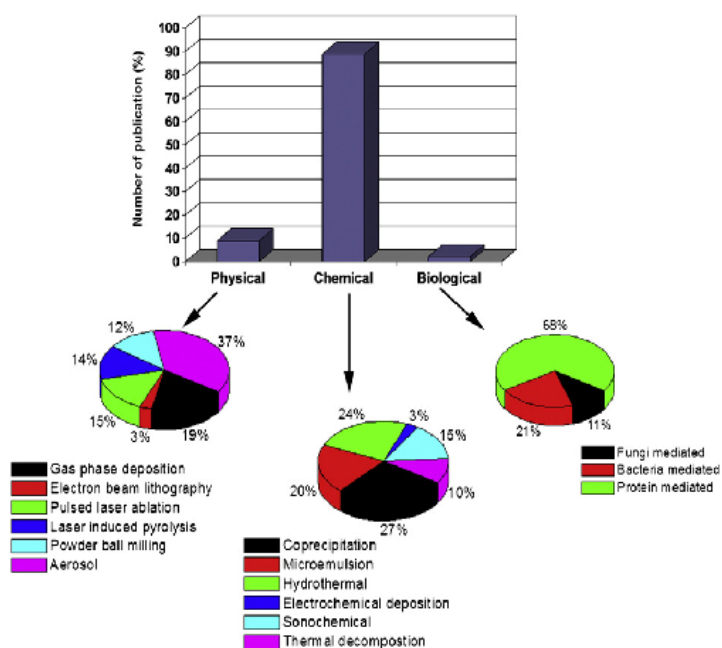
Figure 2.13: Comparison of published work on synthesis of magnetic nanoparticles. [49]

2.2   Synthesis of Magnetic Nanoparticles

Regarding the synthesis of the magnetic NPs, several studies have shown efficient results, the synthesis of magnetic NPs can be done by three classical methods: physical, chemical and biological, among the most important methods from the above cited are: electrochemical mechanisms[43,44], hydrothermal synthesis[45,46], chemical co-precipitation[47], among others. The importance of those methods lies on the accurate control of the variables such as: temperature, concentration, reaction time, and so on. The chemical co-precipitation method, which is the one that our study focus on, involves the dissolution of iron salts controlling the parameters stated before. The control of those parameters may difficult the size controlled synthesis. To reduce the inconvenient, it is possible the addition of coating agents such as Polyvinyl alcohol (PVA)

The three methods named previously are known as routes, and depending on the chosen route the effect on size, shape, size distribution and surface chemistry of the nanoparticles synthesized will change[48]. **Figure** 2.13 shows an assemblage done by *Mahmoudi, et al.* and it presents the different routes to synthesize iron oxides nanoparticles and its derivatives versus the amount of studies done for each method until 2010[49]. The most used method according to **Figure** 2.13 is the co-precipitation method, which in its turn belongs to a chemical method. The facility, low cost and efficiency of co-precipitation are the basis of being the most used method to synthesize magnetic NPs.

2.2.1 Chemical Co-precipitation

The co-precipitation method basically is a process in which normally soluble compounds are removed from a solution by a precipitate, it is widely used due to its facility to proceed and the low hazardous materials[50]. Also, this process facilitate the preparation of fine, nano-crystallized, high-purity and homogeneous powders of oxides[51]. The most important steps on co-precipitation are the nucleation and crystal growth for the formation of solids[49].

There are four reported types of co-precipitation: surface adsorption, occlusion, mechanical entrapment and mixed-crystal formation[52]. Occlusion and mechanical entrapment are said to be product of kinetics of crystal growth, in the other hand surface adsorption and mixed-crystal formation are equilibrium process. This latter process involves the participation of two salts where one of the ions in the crystal lattice of a solid might be replaced by an ion of the another element, furthermore the sizes of those ions do not have to overweight the 5%. Then, the formation of Fe_3O_4 nanoparticles belongs to the mixed-crystal co-precipitation[53].

The formation of Fe_3O_4 by co-precipitation can present the next reactions:

$$Fe^{2+} + 2O^-H \rightarrow Fe(OH)_2 \tag{2.22}$$

$$Fe^{3+} + 3O^-H \rightarrow Fe(OH)_3 \tag{2.23}$$

$$Fe(OH)_2 + 2Fe(OH)_3 \rightarrow Fe_3O_4 + 4H_2O \tag{2.24}$$
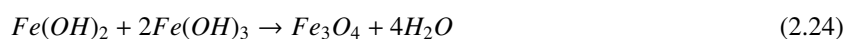
A complete precipitation of magnetite Fe_3O_4 presents a 2:1 molar ratio of $Fe^{+3} : Fe^{+2}$ respectively and its expected pH ranges from 9 and 14[32]. Then, the normal process to follow and to look up is given in **Figure** 2.14.

Nucleation and Crystal Growth

The crystalline formation of many materials from a solution is normally described by the two steps, nucleation and crystal growth, basically the atoms or molecules tend to assemble directly from solution[55]. The size of the particle will truly depend on the factor that predominates in the crystal formation, there are two cases to discuss next, when nucleation predominates and when crystal growth does.

Nucleation is defined as the spontaneous formation of nuclei until a certain point, in such process a minimum number of atoms, ions, or molecules bounds together to form a solid. The process of nucleation has a Gibbs free energy associated ΔG and its expression is $\Delta G = \Delta G_l + \Delta G_s$, the first term corresponds to the surface free energy and the second one to the Gibbs free energy of the transfer crystal grow from solution to bulk solid phase. In a certain point, the addition of those two terms will reach a maximum value due to supersaturation and the size of the particle is called critical size[56].
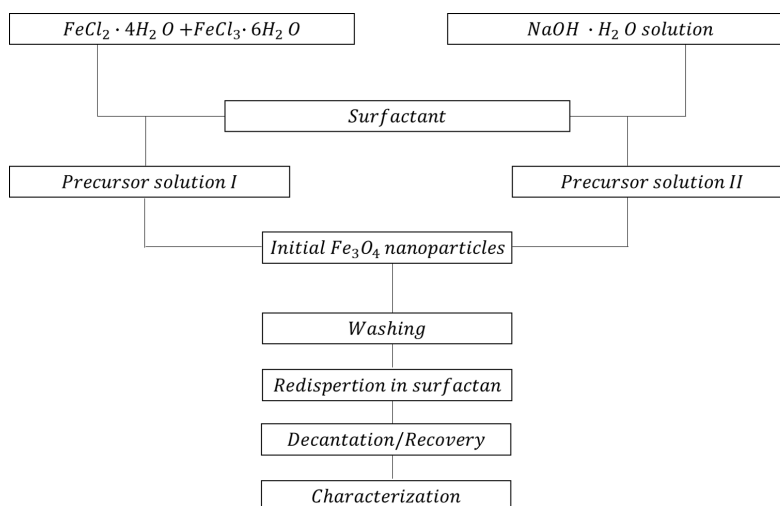
Figure 2.14: Co-precipitation process to form Fe_3O_4 nanoparticles modified from [54].

By contrast, crystal growth occurs after nucleation's and the ions or molecules starts to grow up from the nuclei, where the system starts to be called a crystal. Also, molecules or ions must build into a correct lattice in order to get a ordered system for the crystal to grow. In the case of nucleation predominates, the precipitate will contain a large number of small particles as a result, on the contrary the precipitate will contain a small number of larger particles[53]. In the nanoparticles scenery, both nucleation and crystal might be separated process not intertwined[57]. Furthermore, both processes can be illustrated in the widely known LaMer diagram **Figure** 2.15.[58]
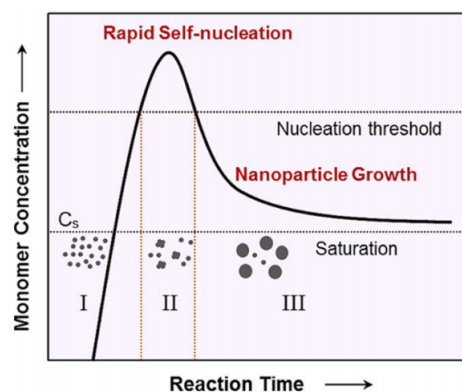
Figure 2.15: LaMer model of the particle nucleation and growth process. [58]
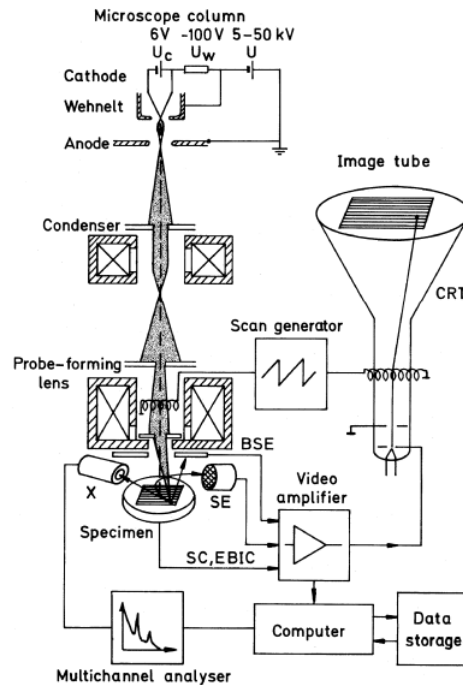
Figure 2.16: Schematic representation of the principle of scanning electron microscope. [59]

2.3   Characterization techniques

2.3.1   Scanning Electron Microscope (SEM)

scanning electron microscopy (SEM), is an electron microscope technique able to produce high resolution images of surface of different materials, is widely used to image and analyze bulk specimens[59]. It uses a high energy focused beam, and released sample backscattered electrons, secondary electrons, and fluorescent X-rays, among others[60]. The working principle of SEM can be interpreted from **Figure** 2.16, basically electrons come out from a cathode and those one are accelerated by a voltage difference produced between the anode and cathode, the voltage difference normally ranges from $0.1\,keV$ and $50\,keV$, which a its turn is known as low-voltage SEM (LVSEM). Electromagnetic lenses will give direction to the electrons (electron beam), by making them pass through a magnetic field provoked by deflection bovines. So that, the electron sweep is possible at the surface of the placed sample, each collision of those electrons at a certain point of the specimen produces secondary electrons (SE), which are going to be detected by an appropriated detector and transformed into an electrical signal; the output signal from the detector controls the intensity of the light emitted by each point of analysis and it will be proportional to the SE emitted from the sample. Then, a computer will show the surface of the sample due to the line by line sampling[61].
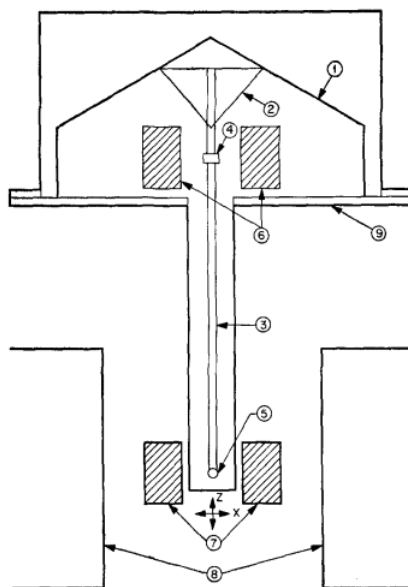
Figure 2.17: Schematic representation of a vibrating sample magnetometer,(1) Loudspeaker transducer. (2) conical paper cup support, (3) drinking straw, (4) permanent magnet reference sample, (5) sample (reference coils) , (7) sample coils, (8) magnet poles, (9) metal container to allow evacuation. [62]

2.3.2 Vibrating-Sample Magnetometer (VSM)

The vibrating sample magnetometer (VSM) is an equipment to perform magnetic characterization of materials (hysteresis, saturation, coercivity and anisotropy). The magnetometer works by a detection of a dipole field form an oscillating magnetic sample which might be placed on a uniform magnetic field[62]. **Figure** 2.17 shows the VSM proposed by *S. Foner*, the operation of this VSM regards on placing a sample in a rod (5: drinking straw), then place the rod vertical to be subjected to a mechanical vibrator (1: Loudspeaker transducer), the rod should be at the center of the pole pieces of an electromagnet (8: magnet poles), where the detection coils (7) are placed. The phenomena lies on the oscillatory motion of the sample will induce a difference of voltage in the detection coil, which will be proportional to the magnetization of the sample.

To get the external magnetic field, some electromagnets with a power supply are placed, in order to measure the produced magnetic field, a Gauss-meter might be used. One important factor regards on the measurement of the magnetic field as a function of the angle, then a bearing rotator and a circular wooden base would complement this. Finally the detection can be done with the coils extracted from electro-mechanical relays. After the signals goes to a computer output to be analyzed[63].
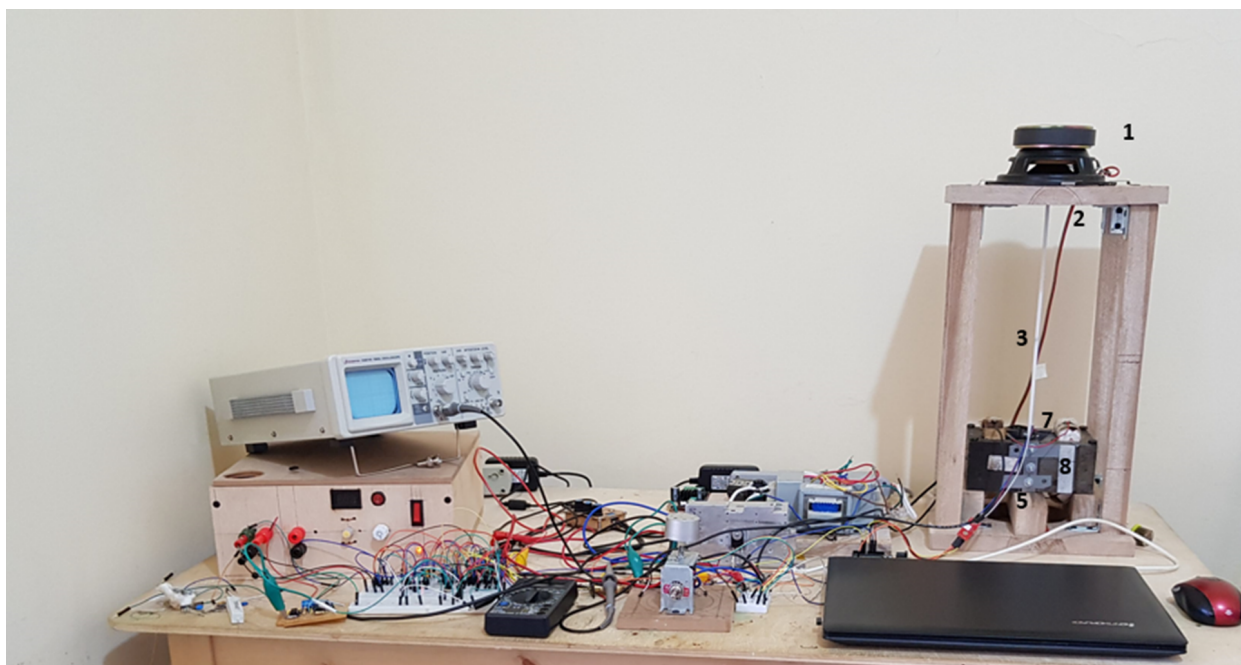
Figure 2.18: Homemade Vibrating-Sample Magnetometer.

For this thesis project, a homemade VSM system, was assembled in Urcuquí-Ecuador and it is shown in **Figure**2.18, the software was controlled with the personal computer, the magnetization values are arbitrary on such system and the induced magnetic field reaches values maximum of 60 mT.

Finally, the samples need to be prepared inside a plastic balloon tube, the tube was cutted exactly to the large needed for the VMS, so that the sample gets inside in a cavity between the electromagnets. The sample preparation is shown in **Figure**2.19, a marker black point indicates where the powder should be, so that the plastic tube needs to be covered by both sides in order to avoid the sample to fall down, the sample was covered with teflon tape.

Figure 2.19: Samples preparation inside a plastic balloon tube.

Chapter 3

Methodology

3.1 Co-precipitation

The principle of the method used in this work lies on a formation of magnetite crystals conformed by ions Fe^{2+} and Fe^{3+}, it consists on mixing in an aqueous dissolution iron salts, in the present study the used salts were ferric chloride $FeCl_3$ and $FeCl_2$; furthermore, the precursor sodium hydroxide $NaOH$ was used, which is vital for co-precipitation due to adequate concentrations of OH^- ion will precipitate both Fe^{2+} and Fe^{3+} ions. Finally, as we previously defined, one way to protect the nanoparticles of a possible oxidation or agglomeration, is the use of coating agents that in the present case was polyvinil alcohol (PVA).

3.1.1 Synthesis of Magnetite Nanoparticles by Co-Precipitation

The synthesis used in this work was the explained co-precipitation method it consisted on using 0.25 M of $FeCl_3 \cdot H_2O$ with 0.125 M of $FeCl_2 \cdot H_2O$. So that, the molar ratio was 2:1 as literature suggests, the temperature was 85 °C, 0.58 M of $NaOH$ was added drop by drop in a 2 seconds delay until get the black coloration (brown/yellow to black), which is the first indicator of getting magnetite ferrofluid as shown in **Figure**3.1. 0,58 M of PVA was added in each solution. The process was done with constant stirring with different reaction times. To follow one of the objectives of the present study, which involves having magnetite nanoparticles with different size nanoparticles, the first phase of synthesis was done by varying the reaction time as is presented in the **Table**3.1.

Finally, 50 mL of each sample were obtained in a ferrofluid state, to posterior magnetic decantation by using strong magnets, the samples were protected from oxidation by placing them in flask covered with aluminium and safely kept to proceed with the calcination.

Sample	Reaction Time (h)	Calcination Time (h)	Temperature (C)
1	0.25	2	200
2	1	6	200
3	2	4	200
4	4	8	200
5	8	2	200

Table 3.1: Reaction and calcination time of PVA-magnetite nanoparticles
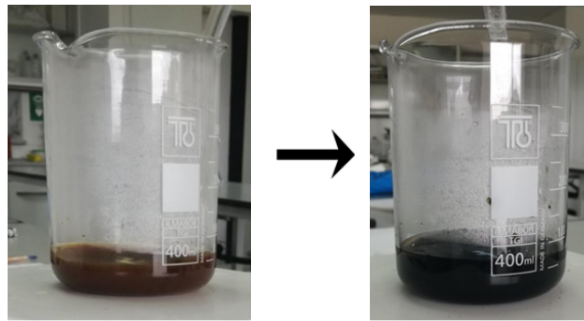
Figure 3.1: Coloration from magnetite nanoparticles synthesis, before and after heating/stirring.

3.1.2   Calcination Process

The calcination process consists on placing different samples to high temperatures so that we can evaporate different substances non-desirable as water, the apparatus used was an oven with 200 °C, the calcination process also can interferes on the size particle, so that we also varied the time of calcination by the same way of reaction time, the same five samples were calcinated in different times with the same 200 °C temperature. The calcination times are given in **Table**3.1.

3.2   Mixtures

The central point of the current thesis project, lies on this section. The mixtures are basically as the names indicates, mixtures of different powders containing in our case, magnetite nanoparticles. The purpose to follow is to observe the change in coercivity and/or shape of hysteresis loops as a function of the mixtures. *P. Bean* in its study[26], considered a range of three different size particles: very small particles single domain with a magnetic behaviour of superparamagnetism or similar to that, single domain nanoparticles large enough that they do not equilibrate and finally large particles with multidomain behaviour.

To make the mixtures is important the concept of proportion, which basically consists on weighing different

	M_5 (g)	M_2 (g)	**Proportion**
Mixture 1	0.021	0.021	1:1
Mixture 2	0.036	0.014	2.6:1
Mixture 3	0.057	0.011	5.2:1
Mixture 4	0.048	0.01	4.8:1

Table 3.2: Proportion mixtures of samples 5 and 2, respectively.

amounts of mass for each sample, then we will have our samples divided in small quantities; proportion roots on having two samples, let us consider the weighed samples A and B, if sample A is one-half of sample B (in terms of mass), then the proportion would be 1:2, the proportions are not always entire numbers but fractional ones. A minimum of two samples are required to perform mixtures, so that samples A and B will be carefully chosen to study their magnetic properties. The aim of performing mixtures lies on obtaining a different magnetic behaviour from two samples (each one magnetically different), the study done by *P. Bean*[26] performs mixtures between SD and MD nanoparticles, then we did mixtures of two samples relatively similar to the ones from Bean's study, which are **Sample 2** and **Sample 5** (see Figures 4.5 and 4.6), in different proportions as is shown in **Table**3.2. Another important point to take into account, is the amount of sample needed by the VSM, to get measurements, the samples were measured from a range 0.01 to 0.1 g.

The procedure to do the mixture was a list of steps detailed next:

- Weight different masses of all the samples to get a high distribution of proportion.

- Select two samples to do the measurements, according to its magnetic response or literature.

- Use a clean container and deposit the two samples.

- Mix the samples with a vigorous agitation.

- Place the final mixture in the plastic balloon tube to perform magnetic measurements.

- Save carefully the samples.

Finally, four Mixtures (Mixture 1, Mixture 2, Mixture 3 and Mixture 4) with different size proportion were performed, their magnetic curves H-M are analyzed and the measurements of coercivity/relative remanence were also taken by checking the software adapted to the homemade VSM. The results are discussed in next section.

Chapter 4

Results & Discussion

4.1 Nano-powders

After the drying process, which in the current study was calcination, it was possible to obtain five different samples in a powder state. **Figure** 4.1 shows the five different magnetite nanoparticles obtained after co-precipitation method, the five samples shown a)-e) corresponds to samples in **Tables** 3.1, with one exception, which is sample f), this one was performed in order to test ten hours of calcination, and the result was a big and hard sample. The different powders shows a black coloration which is indicator of having magnetite nanoparticles.

4.2 SEM Micrographs

The SEM images of samples 1 and 5 are presented in in **Figures** 4.2 and 4.3. It is possible to notice that results until 50 μm shows agglomerates of magnetic nanoparticles, the used SEM could not reach nanometer scale, so for this reason it is not possible to estimate the size of nanoparticles in a completely precise way. Other techniques as TEM or X-ray diffraction can be used to estimate the size of nanoparticles, instead the SEM micrographs present surface morphology of the magnetite powders.

Both results give us a clear comprehension that even if the size of nanoparticles may change, it is not possible to estimate it with the presented SEM micrographs. However, the SEM micrographs show a little points the tendency of magnetite nanoparticles to join together in a cluster-formation as *Briceño, et. al* suggest. The agglomeration is a consequence of the annealing temperature, as it increases, the grain will increase also[64]. Furthermore, this agglomeration is due to Van Der Waals forces between the particles[65].

By comparing the 4.2 with 4.3 figures, it is plausible to infer that the approximate size of agglomerates changes, in the **Figure** 4.2, which is the micrograph of the sample 1 of magnetite, is lower than in the other **Figure** 4.3
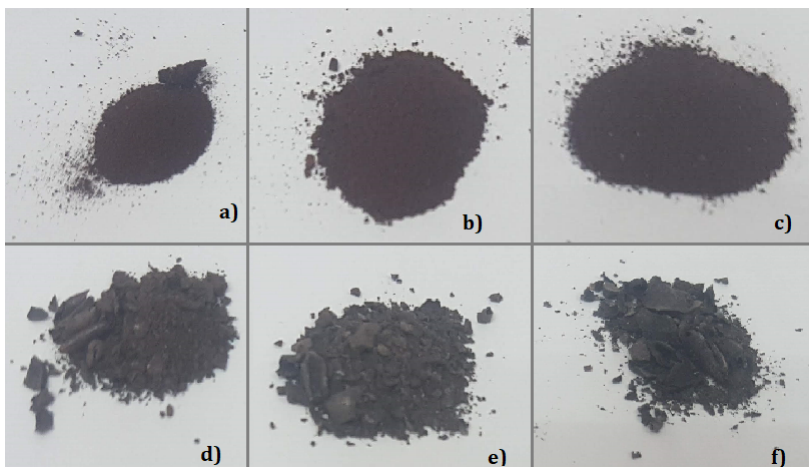
Figure 4.1: Magnetite Fe_3O_4 shown in nanoparticles, a) to e) corresponds to sample 1 to 5.
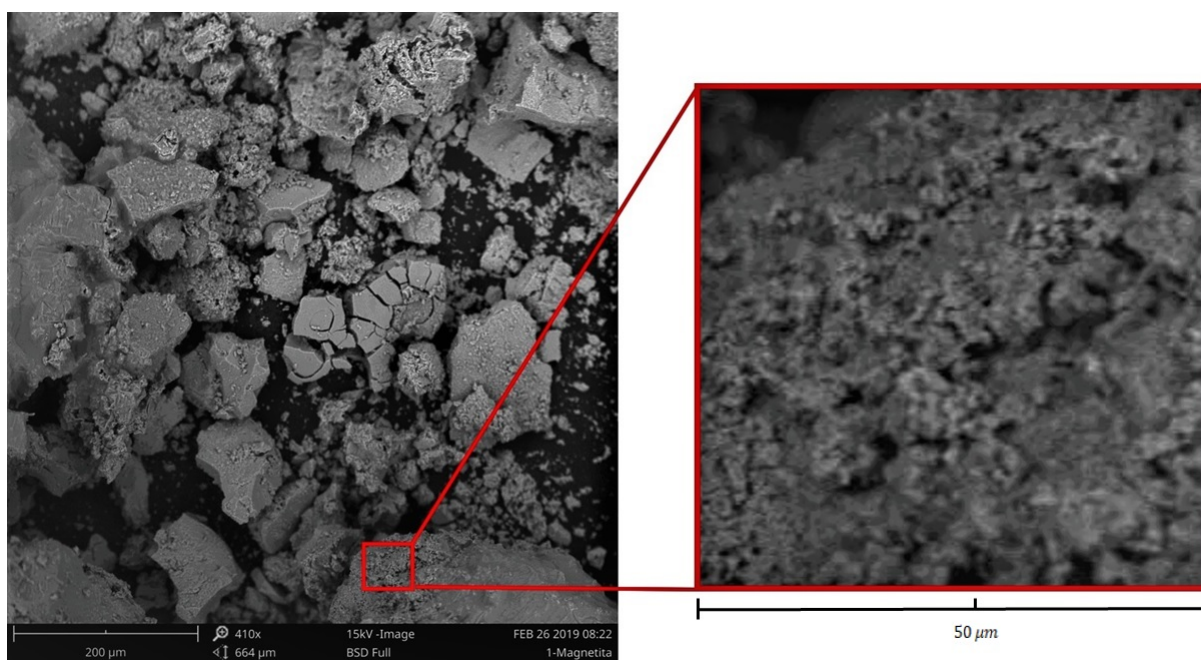

Figure 4.2: SEM micrographs of 15 min. oven dry at 200 C of magnetite NPs (Sample1).
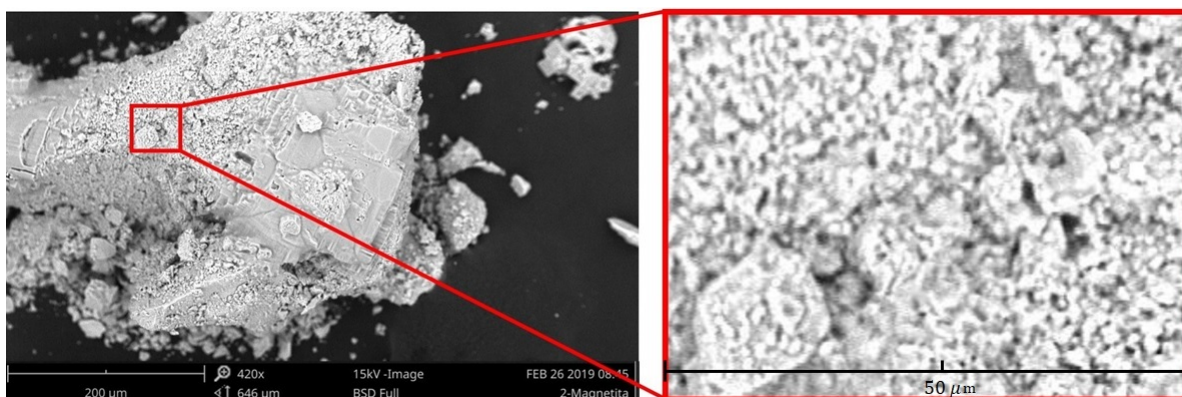
Figure 4.3: SEM micrographs of 8 h. oven dry at 200 C of magnetite Nps (Sample5).

correspondent to sample 5, the main difference between those samples is the reaction time, in the first case the sample was immediately retired from reaction (15 minutes) whereas the second case the sample was left to react along eighth hours (8h).

4.3 Hysteresis Loops

The results of the measurements of VSM are shown in **Figures** 4.4,4.5 and 4.6. All the magnetization curves show hysteresis loops, this indicates the presence of single domain and/or multi domain particles. Nevertheless, it is not possible to assume the absence of superparamagnetic nanoparticles. The axis of magnetization is on arbitrary units because of lack of calibration of VSM and it did not present inconveniences because our purposes were still the shape of hysteresis and measurements of the coercivities. The measurements were taken at low external magnetic field, which provide us the study of the different curves in a field of H maximum of 60 mT where the curves tend to abruptly change.

4.3.1 Sample 1, Sample 3 and Sample 4

The results of the magnetization curve as a function of the applied external field for samples 1,3 and 4 are shown in **Figure**4.4, it is possible to establish a similarity between sample 3 and 4, but it is not trivial to extend this similarity to sample 1, even if the curve of this sample may look as a diamagnetic material due to the loop's tendency to grow against the ferro/ferrimagnetic hysteresis loops, there is another possible explanation to this phenomena and it is related with the imprecision of measurements taken to sample 1, the excess of noise can be the consequence. In contrast, sample 2 and sample 5 show different hysteresis shapes.

Samples M1, M3 and M4, present hysteresis at the arms of its magnetization curves, and there is low remanence. The double loops shape of the samples, each at the end of the arms of hysteresis, indicates the presence of a more complex mechanism for the internal magnetic moments. A model such as the presented here in **Section** (2.1.2) can be used to explain the hysteresis by assuming that the single-domain nanoparticles present antiferromagnetic coupling, i.e, an internal structure of core-shell maybe is present. Another potential possibility regards on the use of PVA as a coating agent, after the calcination process the PVA could not entirely disappear and as a consequence it remains as a shell covering the nanoparticles. In that sense the model simulates the presence of two loops in the arms. In this case, the results of hysteresis at low magnetic field varies against the presented in literature[66,67], where the magnetite nanoparticles presents superparamagnetic behaviour.

The results of hysteresis for each sample are compared with a hysteresis simulation, where such simulation is based on considering the energy of a system with two contributions as is shown in **Eq.**2.18. The simulation considers two magnetic moments, one of them indicates the core magnetization whereas the second represents the shell magnetization. This type of simulation is used to explain the hysteresis in core/shell systems as is reported by *Barrero-Moreno, Et al.* [68]. The parameters in the simulation are varied according the kind of hysteresis presented for each sample.

The samples measurements indicate that the Fe_3O_4 , due to the synthesized Fe_3O_4 NPs have a diameter smaller than 25 nm, which is the critical threshold of Fe_3O_4[69]. The current samples were prepared to realize mixtures because the magnetic properties of each sample are not widely studied and at low magnetic field, normally to perform mixtures the magnetic properties need to be strong single-domain, superparamagnetic or multidomain.

4.3.2   Sample 2

The magnetic hysteresis measurement of sample 2 is presented in **Figure**4.5. The M-H curve evidence a loop hysteresis very closed, the arms of the hysteresis shows an aperture at -40/40 mT, due to the core-shell effect takes place in the Fe_3O_4 nanoparticles.

Both apertures at the arms of the M-H curve are reproduced with the core-shell simulation based on **Eq.**2.18, the right side of **Figure**4.5 is the simulated hysteresis that presents both apertures.

High-frequency hysteresis loops for magnetite nanoparticles at low fields around 14 nm, shows almost linear dependency of magnetization against external magnetic field, furthermore the results of those loops are non-saturated in a range of 60 mT[70]. **Figure** 4.5 shows the same tendency in the curve M-H to grow almost linear as *Morales. et al*, the behaviour is almost superparamagnetic but it still has hysteresis at the arms. In the second case, the non-saturated curves are not present in **Figure** 4.5 because the size distribution of sample 2 of magnetite nanoparticles may not match with the 14 nm NPs presented in other studies.
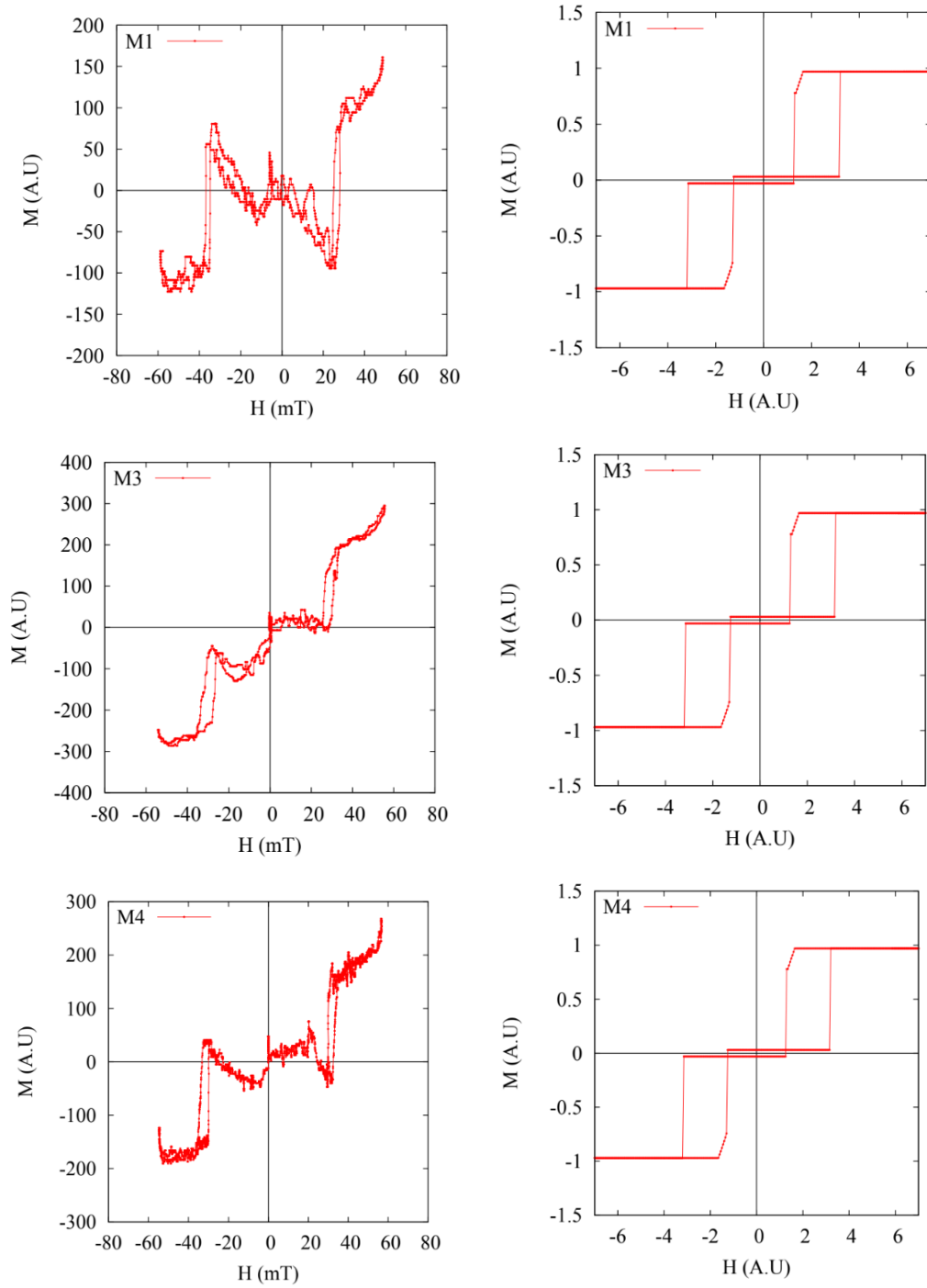
Figure 4.4: Left figures: hysteresis loops of magnetite nanoparticles, samples 1,3,4 taken in homemade VSM. Right figures: simulated hysteresis loops for each sample 1,3,4

In order to make the mixtures, several studies [26,71] have tested a mixture between single-domain nanoparticles and multi-domain nanoparticles, most of the proportion are 1:1. Then, sample 2 is a good candidate to perform mixture due to its single-domain behaviour. It is important to remark that the assemble of nanoparticles may present some particles in superparamagnetic state.
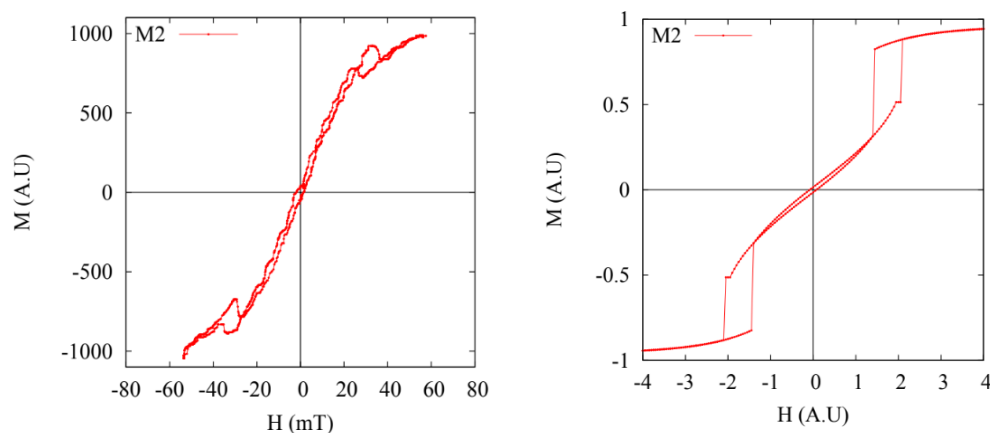

Figure 4.5: Left figure: hysteresis loop of magnetite nanoparticles, sample 2 taken in homemade VSM. Right figure: simulated hysteresis loop for sample 2.

4.3.3 Sample 5

The VSM measurement of sample 5, is shown in left side of **Figure**4.6. The current sample have particles greater than sample 2 ,due to crystal growth should predominate against nucleation in the formation of Fe_3O_4 NPs, for that reason the reaction time is larger (8h) than in the other synthesized samples.

The shape in the hysteresis of sample 5, which is a loop, present an evidence of having particles between multi-domain particles and single-domain states, with a big probability of having "blocked nanoparticles" and it is a perfect candidate to perform mixtures with the already explained sample 2. As in sample 2, sample 5 have a change in the hysteresis making it closer at -20/20 mT, once again this change in the M-H curve is due to core-shell effect as is it evinced by the simulation showed in the right side of **Figure**4.6.

Several studies in low field magnetic hysteresis loops also present similar results as the ones shown in **Figure**4.6. *Morales. et al*, proposes that bigger magnetite nanoparticles around 35nm shows hysteresis in almost ellipsoidal shapes, where the areas becomes higher as well as the H field increases, in this case the saturation magnetization $\mu_0 H = 60mT$ [70]. Comparing with the results of sample 5, there is an increment in area as the H field goes away from

zero, this could be a proof that the size of nanoparticles of sample 5 are bigger or at least are around 35 nm.
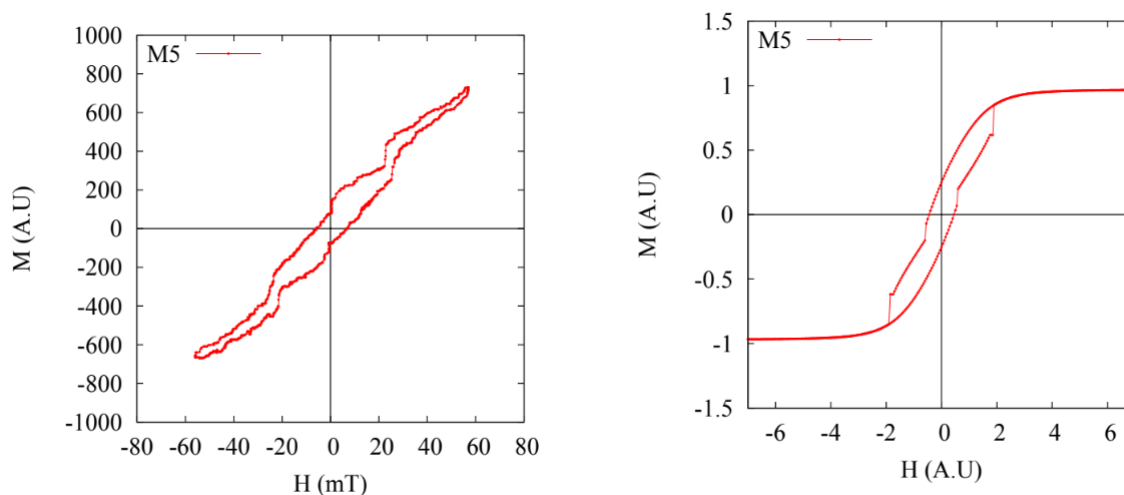

Figure 4.6: Left figure: hysteresis loop of magnetite nanoparticles, sample 5 taken in homemade VSM. Right figure: simulated hysteresis loop for sample 5.

4.4 Mixtures: Sample 5 and Sample 2

Once both samples (5,2) were selected by the reason explained above, the samples were subjected to a mixing procedure by changing the proportion as it is shown in **Table**3.2. The four VSM measurements are shown in **Figures** 4.7, 4.9, 4.9 and 4.11 , and it is possible to confirm a difference in the hysteresis shape for each mixture due to the change in the proportion.

Mix(1) in **Figure**4.7 shows an hysteresis loop of a proportion 1:1 between sample 2 and sample 5, the resulting shape of hysteresis exhibit a contraction in the center of hysteresis, very similar to the one presented in wasp-waists hysteresis loop. A mixture with a soft magnetic material and a hard material give us as a result a wasp-waisted hysteresis loop as [37] predicted. Another study [26], also confirms the modification on hysteresis loops as the population SD-MD are mixed.

Comparing the results obtained of WWHL, there are some models explained by *De la Torre. et al* that proposes the WWHL as a result of exchanging coupling between a soft magnetic material (ferrimagnetic) and a hard material which can present big remanences and coercivities, those materials and the addition of a parameter called exchange-parameter, σ, give us as a result a variety of loops shown in **Figure** 4.8. So that, mixing two different magnetic behaviours may end up with a change in the total magnetic behaviour of the composite, in the current case the result
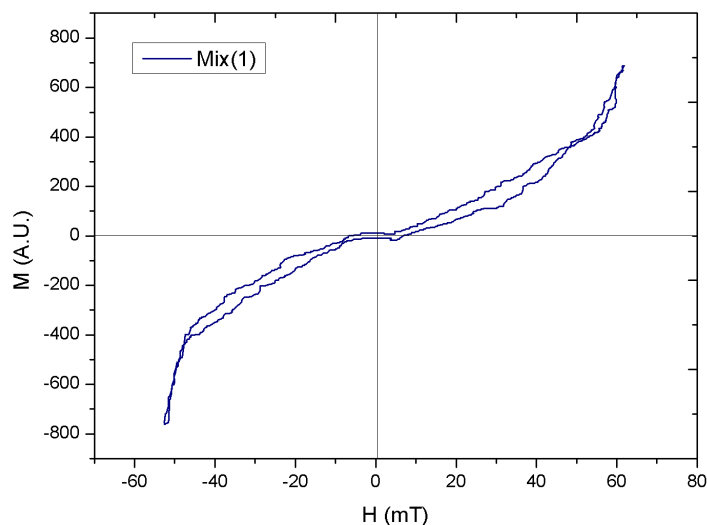
Figure 4.7: Low field VSM hysteresis loops for mixture 1 (Mix1) of magnetite nanoparticles.

was a WWHL as is shown in **Figure** 4.7.

Mix(2) can not be catalogued neither as wasp-waisted hysteresis loops (WWHL) or potbellies hysteresis loop (PHL) but it has differences on coercivities as it is shown in **Table**4.1, additionally there exist a variation in the shape of hysteresis loops due to the proportion of samples 5 and 2. The results show that there is a magnetization linear growing as well as the field H is increased, this result is related with the study of **Morales. et al** and its relation with having non-saturated loops presented by magnetite nanoparticles of low sizes (15 nm). Also, the arms of the loop present a decrease on remanence at around 50 mT.

Mix(3) and Mix(4) present an increment in its center of hysteresis making it to be similar to a potbellied hysteresis loop, by taking the simulation of *Tauxe, Et Al.*[9] in order to have a PHL it is necessary to mix a distribution of single-domain nanoparticles and superparamagnetic ones. Then both samples could have some amount of both single domain and superparamagnetic particles. Due the synthesis, calcination process, coercitivities values and hysteresis shapes of samples 2 and 5, the more realistic assumption is that sample 2 have a particle distribution of single domain and superparamagnetic particles. This assumption can explain the very closed hysteresis of the loop due the amount of superparamagnetic particles in to the sample 2. For that reason the shape of potbelly is achieved.
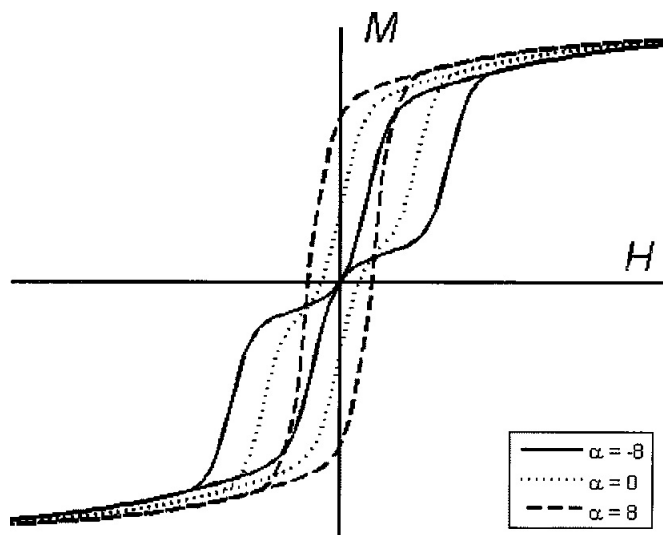
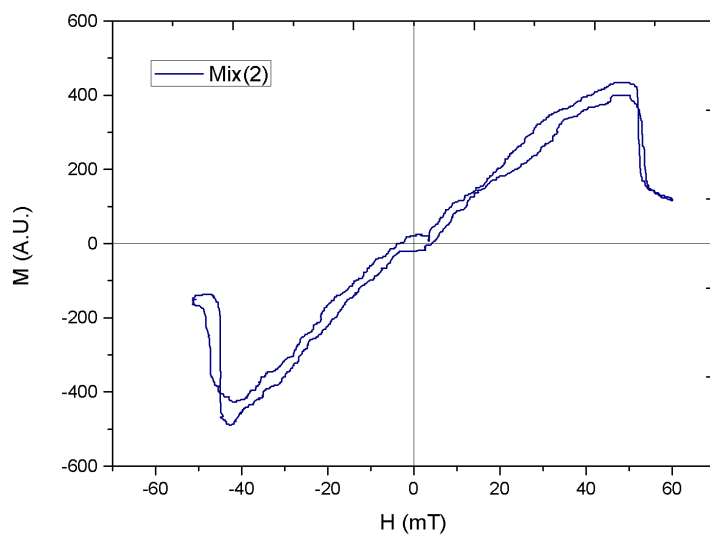Figure 4.8: Effect of σ exchange-parameter on wasp-waist model. [37]

Figure 4.9: Low field VSM hysteresis loops for mixture 2 (Mix2) of magnetite nanoparticles.
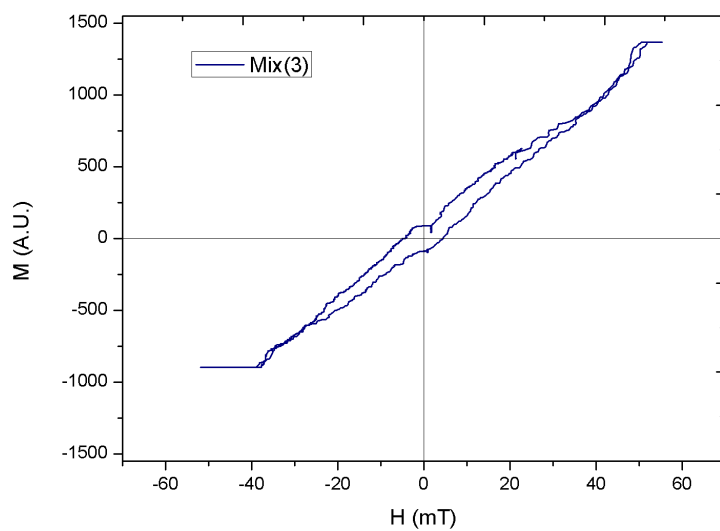
Figure 4.10: Low field VSM hysteresis loops for mixture 3 (Mix3) of magnetite nanoparticles.
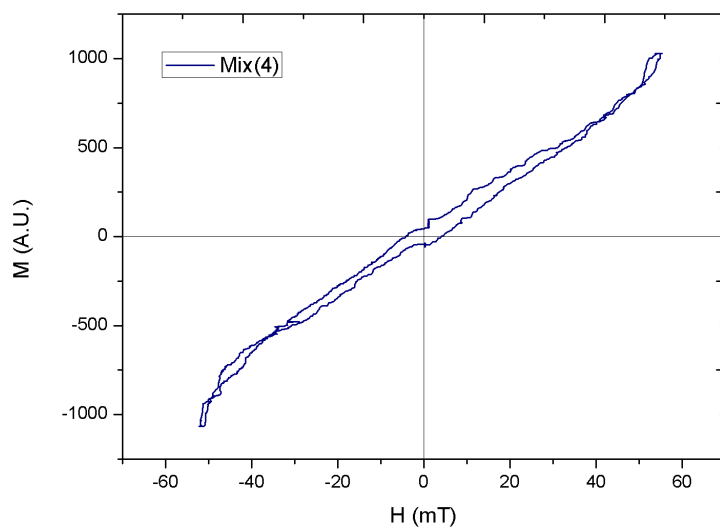

Figure 4.11: Low field VSM hysteresis loops for mixture 4 (Mix4) of magnetite nanoparticles.

4.5   Coercivity change in Mixtures

Mixture	H_{c1} (mT)	H_{c2} (mT)	H_c (mT)
Mix 1	6.87	-6.61	6.74
Mix 2	4.13	-4.00	4.065
Mix 3	4.40	-4.61	4.505
Mix 4	4.06	-4.06	4.06
M2	4.55	-1.82	1.685
M5	9.80	-4.21	7.01

Table 4.1: Coercivity values taken from VSM measurements of mixtures magnetite nanoparticles.

In order to change both coercive values of hysteresis loops and also its shapes, mixtures between sample 2 and 5 were carried out. The change in the coercivity is expected to decrease as the amount of sample 5 is reduced. Three different curves of change in coercivity values can be obtained, those are show in detail in works done previously[71],[26][72]. The changes in coercivity values (H_c) for the different mixtures are given in **Table**4.1, it is notable that all coercive values H_c are different between them, and in the case of the mixtures this is due of the change in proportion mentioned before.

In order to analyze the variation of coercivity as a function of mass change, which is a consequence of change in proportion, the relation $RPM_2 = M_5(g)/M_5(g) + M_2(g)$ is used, here RPM_2 is the relative percentage of sample 2 in the mixtures, and M_5 and M_2 are the mass values of each sample. The previous relation compares proportions used and how does the proportion affects to the coercivity values. **Figure**4.12 plots the results of RPM_2 as a function of coercivity values H_c.

The plots of **Figure** 4.12 shows the tendency of H_c to decrease as M_5 decreases as it is expected and previous works[71],[26][72] have tested this decreasing. For the results obtained the behaviour corresponds to mixtures of single domain with multidomain particles, which produces different total magnetic behaviour as WWHL or pot-bellied hysteresis loops, i.e, the amount of superparamagnetics particles present on the mixture do not affect the major behavior.
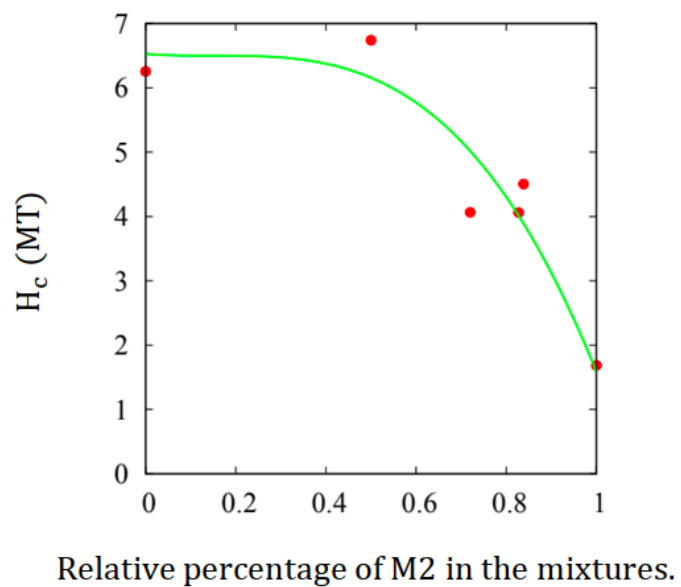
Figure 4.12: Coercivity values as a function of relative percentage of sample 2 in mixtures. The green line shows the visual behaviour of the measurements.

Chapter 5

Conclusions

Wasp-waists and Potbellies hysteresis loops were obtained through a mixture between populations of magnetite (Fe_3O_4) nanoparticles, the mixtures were performed under a principle of proportion-mixture, this latter corresponds to a set of different size nanoparticles. Basically, the mixtures used two different samples (5 and 2) because those ones presented states of interest on mixtures: single-domain with a strong response and multi-domain relatively similar to blocked state nanoparticles. The Fe_3O_4 NPs were synthesized by co-precipitation method, so that the set of different sizes consisted of varying the parameters of co-precipitation such as the reaction and calcination times.

Both characterization techniques (SEM) and (VSM) provide us information about the structural and magnetic properties of the Fe_3O_4 nanoparticles, the former technique (SEM) confirmed such nanoparticles to be in an agglomerated state, whereas through the VSM, it was possible to obtain different hysteresis loops; after a mixture process, this technique allowed us to obtain wasp-waisted and potbellied hysteresis loops. Furthermore, the results of measuring the coercivity values were proof of the change in those values with a change in proportion mixtures.

The present thesis project opens the door to further research in the scope of synthesizing and mixing magnetic nanoparticles in order to study the magnetic properties of different materials with aims of future applications in the different fields that nanotechnology offers.

Bibliography

[1] Pankhurst, Q. A.; Connolly, J.; Jones, S.; Dobson, J. Applications of magnetic nanoparticles in biomedicine. *Journal of physics D: Applied physics* **2003**, *36*, R167.

[2] Black, C. T.; Gates, S. M.; Murray, C. B.; Sun, S. Magnetic storage medium formed of nanoparticles. 2000; US Patent 6,162,532.

[3] Sahoo, Y.; Goodarzi, A.; Swihart, M. T.; Ohulchanskyy, T. Y.; Kaur, N.; Furlani, E. P.; Prasad, P. N. Aqueous ferrofluid of magnetite nanoparticles: fluorescence labeling and magnetophoretic control. *The Journal of Physical Chemistry B* **2005**, *109*, 3879–3885.

[4] Wu, W.; He, Q.; Jiang, C. Magnetic iron oxide nanoparticles: synthesis and surface functionalization strategies. *Nanoscale research letters* **2008**, *3*, 397.

[5] Frenkel, J.; Doefman, J. Spontaneous and induced magnetisation in ferromagnetic bodies. *Nature* **1930**, *126*, 274.

[6] Akbarzadeh, A.; Samiei, M.; Davaran, S. Magnetic nanoparticles: preparation, physical properties, and applications in biomedicine. *Nanoscale research letters* **2012**, *7*, 144.

[7] Stoner, E. EC Stoner and EP Wohlfarth, Philos. Trans. R. Soc. London, Ser. A 240, 599 (1948). *Philos. Trans. R. Soc. London, Ser. A* **1948**, *240*, 599.

[8] Bedanta, S. Supermagnetism in magnetic nanoparticle systems. Ph.D. thesis, Verlag nicht ermittelbar, 2006.

[9] Tauxe, L.; Mullender, T. A. T.; Pick, T. in Magnetic Hysteresis. **1996**, *101*, 571–583.

[10] Weiss, P. The hypothesis of the molecular field and the property of ferromagnetism. *J. de Phys. Rad* **1907**, *6*, 661–690.

[11] Weinberg, S. *The quantum theory of fields*; Cambridge university press, 1995; Vol. 2.

[12] Oĥandley, R. C. Soft magnetic materials. *Modern Magnetic Materials* **2000**,

[13] Minnesota, Classes of Magnetic Materials. http://www.irm.umn.edu/hg2m/hg2m$_b$/$hg2m_b$.$html$/ (accessed March 21, 2019).

[14] Banerjee, S. K.; Moskowitz, B. M. *Magnetite biomineralization and magnetoreception in organisms*; Springer, 1985; pp 17–41.

[15] Chikazumi, S.; Graham, C. D. *Physics of Ferromagnetism 2e*; Oxford University Press on Demand, 2009; Vol. 94.

[16] Li, Q.; Kartikowati, C. W.; Horie, S.; Ogi, T.; Iwaki, T.; Okuyama, K. Correlation between particle size/domain structure and magnetic properties of highly crystalline Fe 3 O 4 nanoparticles. *Scientific reports* **2017**, *7*, 9894.

[17] Peddis, D.; Cannas, C.; Musinu, A.; Piccaluga, G. Magnetism in nanoparticles: beyond the effect of particle size. *Chemistry–A European Journal* **2009**, *15*, 7822–7829.

[18] Tannous, C.; Gieraltowski, J. The Stoner–Wohlfarth model of ferromagnetism. *European journal of physics* **2008**, *29*, 475.

[19] E.Y.Tsymbal, Magnetic properties of materials. https://unlcms.unl.edu/cas/physics/tsymbal/teaching/SSP-927/Section%2016$_{magnetic properties_2}$.pdf (accessed March 31, 2019).

[20] Tobia, D.; De Biasi, E.; Granada, M.; Troiani, H.; Zampieri, G.; Winkler, E.; Zysler, R. Evolution of the magnetic anisotropy with particle size in antiferromagnetic Cr 2 O 3 nanoparticles. *Journal of Applied Physics* **2010**, *108*, 104303.

[21] Salazar-Alvarez, G.; Sort, J.; Surinach, S.; Baró, M. D.; Nogués, J. Synthesis and size-dependent exchange bias in inverted core- shell MnO| Mn3O4 nanoparticles. *Journal of the American Chemical Society* **2007**, *129*, 9102–9108.

[22] Nogués, J.; Schuller, I. K. Exchange bias. *Journal of Magnetism and Magnetic Materials* **1999**, *192*, 203–232.

[23] Sun, X.; Frey Huls, N.; Sigdel, A.; Sun, S. Tuning exchange bias in core/shell FeO/Fe3O4 nanoparticles. *Nano letters* **2011**, *12*, 246–251.

[24] Kavich, D.; Dickerson, J.; Mahajan, S.; Hasan, S.; Park, J.-H. Exchange bias of singly inverted FeO/Fe 3 O 4 core-shell nanocrystals. *Physical Review B* **2008**, *78*, 174414.

[25] Bean, C.; Livingston, u. D. Superparamagnetism. *Journal of Applied Physics* **1959**, *30*, S120–S129.

[26] Bean, C. Hysteresis loops of mixtures of ferromagnetic micropowders. *Journal of Applied Physics* **1955**, *26*, 1381–1383.

[27] Weil, L.; Gruner, L.; Deschamps, A. Orientation des précipitations du cobalt dans un alliage CuCo. *COMPTES RENDUS HEBDOMADAIRES DES SEANCES DE L ACADEMIE DES SCIENCES* **1957**, *244*, 2143–2146.

[28] Knappwost, A. Kollektivparamagnetismus und volumen magnetisierter aerosole. *Zeitschrift für Elektrochemie, Berichte der Bunsengesellschaft für physikalische Chemie* **1957**, *61*, 1328–1334.

[29] Hahn, R. R. Hahn and E. Kneller, Z. Metallkd. 49, 426 (1958). *Z. Metallkd.* **1958**, *49*, 426.

[30] Berkowitz, A. AE Berkowitz and PJ Flanders, J. Appl. Phys. Suppl. 30, 111S (1959). *J. Appl. Phys. Suppl.* **1959**, *30*, 111S.

[31] Cornell, R. M.; Schwertmann, U. *The iron oxides: structure, properties, reactions, occurrences and uses*; John Wiley & Sons, 2003.

[32] Gupta, A. K.; Gupta, M. Synthesis and surface engineering of iron oxide nanoparticles for biomedical applications. *biomaterials* **2005**, *26*, 3995–4021.

[33] Kurti, N. *Selected works of louis neel*; CRC Press, 1988.

[34] Enriquez-Navas, P. M.; Garcia-Martin, M. L. *Frontiers of Nanoscience*; Elsevier, 2012; Vol. 4; pp 233–245.

[35] Borisenko, V. E.; Ossicini, S. *What is what in the Nanoworld: A Handbook on Nanoscience and Nanotechnology*; John Wiley & Sons, 2013.

[36] Roberts, A. P.; Cui, Y.; Verosub, K. L. Wasp-waisted hysteresis loops: Mineral magnetic characteristics and discrimination of components in mixed magnetic systems. *Journal of Geophysical Research: Solid Earth* **1995**, *100*, 17909–17924.

[37] Bennett, L. H.; Della Torre, E. Analysis of wasp-waist hysteresis loops. *Journal of applied physics* **2005**, *97*, 10E502.

[38] Wasilewski, P. J. Magnetic hysteresis in natural materials. *Earth and Planetary Science Letters* **1973**, *20*, 67–72.

[39] Huang, M.-Q.; Hsu, Y.-N.; McHenry, E.; Laughlin, D. Soft magnetic properties of nanocrystalline amorphous HITPERM films and multilayers. *IEEE transactions on magnetics* **2001**, *37*, 2239–2241.

[40] Moser, A.; Berger, A.; Margulies, D. T.; Fullerton, E. E. Biquadratic coupling in antiferromagnetically coupled magnetic recording media. *Journal of applied physics* **2004**, *95*, 6657–6659.

[41] Sebt, A.; Akhavan, M. Switching field distribution of magnetic fine particles. *Journal of magnetism and magnetic materials* **2001**, *237*, 111–118.

[42] Chantrell, R.; O'Grady, K. Magnetic characterization of recording media. *Journal of Physics D: Applied Physics* **1992**, *25*, 1.

[43] Cabrera, L.; Gutierrez, S.; Menendez, N.; Morales, M.; Herrasti, P. Magnetite nanoparticles: electrochemical synthesis and characterization. *Electrochimica Acta* **2008**, *53*, 3436–3441.

[44] Fajaroh, F.; Setyawan, H.; Widiyastuti, W.; Winardi, S. Synthesis of magnetite nanoparticles by surfactant-free electrochemical method in an aqueous system. *Advanced Powder Technology* **2012**, *23*, 328–333.

[45] Daou, T.; Pourroy, G.; Bégin-Colin, S.; Greneche, J.; Ulhaq-Bouillet, C.; Legaré, P.; Bernhardt, P.; Leuvrey, C.; Rogez, G. Hydrothermal synthesis of monodisperse magnetite nanoparticles. *Chemistry of Materials* **2006**, *18*, 4399–4404.

[46] Haw, C. Y.; Mohamed, F.; Chia, C. H.; Radiman, S.; Zakaria, S.; Huang, N.; Lim, H. Hydrothermal synthesis of magnetite nanoparticles as MRI contrast agents. *Ceramics International* **2010**, *36*, 1417–1422.

[47] Ranjbakhsh, E.; Bordbar, A.; Abbasi, M.; Khosropour, A.; Shams, E. Enhancement of stability and catalytic activity of immobilized lipase on silica-coated modified magnetite nanoparticles. *Chemical Engineering Journal* **2012**, *179*, 272–276.

[48] Jeong, U.; Teng, X.; Wang, Y.; Yang, H.; Xia, Y. Superparamagnetic colloids: controlled synthesis and niche applications. *Advanced Materials* **2007**, *19*, 33–60.

[49] Mahmoudi, M.; Sant, S.; Wang, B.; Laurent, S.; Sen, T. Superparamagnetic iron oxide nanoparticles (SPIONs): development, surface modification and applications in chemotherapy. *Advanced drug delivery reviews* **2011**, *63*, 24–46.

[50] Yuanbi, Z.; Zumin, Q.; Huang, J. Preparation and analysis of Fe3O4 magnetic nanoparticles used as targeted-drug carriers. *Chinese Journal of Chemical Engineering* **2008**, *16*, 451–455.

[51] Zhong, Z.; Li, Q.; Zhang, Y.; Zhong, H.; Cheng, M.; Zhang, Y. Synthesis of nanocrystalline Ni–Zn ferrite powders by refluxing method. *Powder Technology* **2005**, *155*, 193–195.

[52] Kolthoff, I. M.; Elving, P. J. *Treatise on analytical chemistry*; John Wiley & Sons, 1993; Vol. 13.

[53] Skoog, D. A.; West, D. M.; Holler, F. J.; Crouch, S. *Fundamentals of analytical chemistry*; Nelson Education, 2013.

[54] Sun, J.; Zhou, S.; Hou, P.; Yang, Y.; Weng, J.; Li, X.; Li, M. Synthesis and characterization of biocompatible Fe3O4 nanoparticles. *Journal of biomedical materials research Part A* **2007**, *80*, 333–341.

[55] Kashchiev, D. *Nucleation*; Elsevier, 2000.

[56] Nehrke, G. Calcite precipitation from aqueous solution: transformation from vaterite and role of solution stoichiometry. Ph.D. thesis, UU Dept. of Earth Sciences, 2007.

[57] Tartaj, P.; Morales, M.; Veintemillas-Verdaguer, S.; Gonzalez-Carreno, T.; Serna, C. Handbook of magnetic materials. 2006.

[58] Jiang, C. Synthesis, Assembly, and Integration of Magnetic Nanoparticles for Nanoparticle-Based Spintronic Devices. *HKU Theses Online (HKUTO)* **2017**,

[59] Reimer, L. *Scanning electron microscopy: physics of image formation and microanalysis*; Springer, 2013; Vol. 45.

[60] Ford, M.; Nill, M.; Bryant, A. Lab 04: Energy Dispersive Spectrometry in the SEM. 2011.

[61] Egas, D. Microscopía Electrónica: Fundamentos, Teoría y Aplicaciones. 1998.

[62] Foner, S. Vibrating sample magnetometer. *Review of Scientific Instruments* **1956**, *27*, 548–548.

[63] Burgei, W.; Pechan, M. J.; Jaeger, H. A simple vibrating sample magnetometer for use in a materials physics course. *American Journal of Physics* **2003**, *71*, 825–828.

[64] Briceño, S.; Brämer-Escamilla, W.; Silva, P.; Delgado, G. E.; Plaza, E.; Palacios, J.; Cañizales, E. Effects of synthesis variables on the magnetic properties of CoFe2O4 nanoparticles. *Journal of Magnetism and Magnetic Materials* **2012**, *324*, 2926–2931.

[65] Maaz, K.; Mumtaz, A.; Hasanain, S.; Ceylan, A. Synthesis and magnetic properties of cobalt ferrite (CoFe2O4) nanoparticles prepared by wet chemical route. *Journal of magnetism and magnetic materials* **2007**, *308*, 289–295.

[66] Kim, D.; Zhang, Y.; Voit, W.; Rao, K.; Muhammed, M. Synthesis and characterization of surfactant-coated superparamagnetic monodispersed iron oxide nanoparticles. *Journal of Magnetism and Magnetic Materials* **2001**, *225*, 30–36.

[67] Sun, S.; Zeng, H. Size-controlled synthesis of magnetite nanoparticles. *Journal of the American Chemical Society* **2002**, *124*, 8204–8205.

[68] Barrero-Moreno, M.; Restrepo-Parra, E.; Acosta-Medina, C. Hysteresis in Core/Shell Nanowire with Mixed Spin Ising. *Advanced Studies in Theoretical Physics* **2018**, *12*, 281–299.

[69] Wei, Y.; Han, B.; Hu, X.; Lin, Y.; Wang, X.; Deng, X. Synthesis of Fe3O4 nanoparticles and their magnetic properties. *Procedia Engineering* **2012**, *27*, 632–637.

[70] Morales, I.; Costo, R.; Mille, N.; Silva, G. B. d.; Carrey, J.; Hernando, A.; Presa, P. d. l. High Frequency Hysteresis Losses on γ-Fe2O3 and Fe3O4: Susceptibility as a Magnetic Stamp for Chain Formation. *Nanomaterials* **2018**, *8*, 970.

[71] Kneller, E.; Luborsky, F. Particle size dependence of coercivity and remanence of single-domain particles. *Journal of Applied Physics* **1963**, *34*, 656–658.

[72] Meiklejohn, W. H. Experimental Study of the Coercive Force of Fine Particles. *Rev. Mod. Phys.* **1953**, *25*, 302–306.

Abbreviations

AFM antiferromagnetic 12

EB exchange bias 12

FIM ferrimagnetic 12
FM ferromagnetic 12

H magnetic field 1

LVSEM low-voltage SEM 22

MNPs magnetic nanoparticles 1, 5

PHL potbellies hysteresis loop 38
PVA polyvinil alcohol 2, 27

SD single-domain 1, 6
SE secondary electrons 22
SEM scanning electron microscopy 2, 22
SPI superexchange interactions 7
SPM superparamagnetism 2
SW Stoner and Wohlfarth 9

VSM vibrating sample magnetometer 2, 23

WWHL wasp-waisted hysteresis loops 16, 38